Molecular Orientation Distributions in Poly(ethylene terephthalate) Thin Films and Fibers from Multidimensional DECODER NMR Spectroscopy

B. F. Chmelka,† K. Schmidt-Rohr, and H. W. Spiess*

Max-Planck-Institut für Polymerforschung, Postfach 3148, W-6500 Mainz, Germany

Received October 15, 1992; Revised Manuscript Received January 19, 1993

ABSTRACT: Multidimensional DECODER NMR experiments are applied to several industrial samples of poly(ethylene terephthalate) (PET) thin films and fibers, exploiting natural-abundance ^{13}C resonances from different carbon sites to quantify orientational order in these materials. In two-dimensional (2D) DECODER NMR, the sample is flipped through a discrete angle during the mixing time of a 2D exchange NMR experiment. This allows frequencies at two spatial orientations to be correlated to elucidate molecular order in the sample. The theoretical background needed to analyze the corresponding 2D pattern in terms of angular distributions is outlined, and reconstruction of relevant one-dimensional slices through the orientation distribution is demonstrated. In PET fibers, direct reconstruction produces an orientation distribution that is at least bimodal; 60% of the chains are highly oriented, with a full-width-at-half-maximum (fwhm) of 20°. The angle between the phenylene para axis and the fiber axis is determined to be 18 ± 4°. For biaxially drawn films, the direct reconstruction of slices through the orientation distribution shows that in a highly oriented fraction (ca. 80%) of the sample, the chain axes are confined to the film plane (fwhm of 15°), while the in-plane distribution of chain axes is much broader (fwhm of ca. 90°); the phenylene rings and carboxyl group planes are oriented preferentially parallel to the plane of the film (fwhm of 55°). Film samples collected at different points across an industrial sheet of PET are shown to exhibit sizable variations in ordering. For the center of the sheet, a slight preferential orientation along the transverse direction is clearly detected. Increased alignment of the PET chains (fwhm of 55°), with the preferred orientation rotated toward the machine direction, is observed near the sheet edge. In uniaxial films, the fwhm of the orientation distribution is measured to be 85°. A 3D DECODER experiment is implemented to separate frequency patterns that overlap in two dimensions.

I. Introduction

In heterogeneous macromolecular solids, numerous material properties, such as optical response, gas permeability, and tensile or compressive strengths, are influenced by the degree of microstructural ordering in the sample. Underlying orientational order, both at the molecular level and at the level of oriented crystalline domains, exerts a sizable influence on the observed physicochemical properties of polymeric thin films, fibers, and oriented bulk solids.[1] Mechanical manipulation of these materials during processing tends to orient molecular segments and crystallite assemblies. The attendant anisotropy governs many structure-dependent material features that, as a logical consequence, acquire a directional character. In correlating these macroscopic properties with their dependence on preparatory processing conditions, a picture of molecular structure and order in the crystalline, amorphous, and partially ordered regions is of great value. Numerous scattering and spectroscopic techniques are employed to measure orientational order in polymers.[1,2] Nevertheless, the information about higher-order moments of the orientation-distribution function is usually not accessible, with the notable exception of pole-figure analysis in wide-angle X-ray scattering (WAXS).[3] Scattering techniques, however, are largely restricted to the study of crystalline portions of polymers, and in poly(ethylene terephthalate) (PET), which we characterize here by NMR, the analysis of the X-ray patterns is further complicated by the fact that the unit cell is triclinic.[4,5] No low-order reflection for a direction exactly parallel to the PET chain axis is present.[6] Detailed birefringence analysis of biaxial PET films is also rather difficult.[6]

† Present address: Department of Chemical and Nuclear Engineering, University of California, Santa Barbara, CA 93106.

The angular dependences (anisotropies) of nuclear magnetic resonance (NMR) interactions are known to be powerful local probes of molecular orientation.[7,8] Recent ^{2}H NMR lineshape studies, for example, on deuterated poly(ethylene terephthalate) thin films[9] provide insights on the orientational ordering in these materials. Different fractions in the samples were distinguished through differences in relaxation times. However, while ^{2}H NMR is restricted to protonated sites and requires enrichment with deuterium, ^{13}C NMR can probe the orientation of both the protonated and the nonprotonated sites, such as the carboxyl carbons in PET. Morever, the ^{13}C NMR results to be presented here and the ^{2}H NMR study on deuterated PET films yield complementary information, as the principal axes of the anisotropic NMR interactions of the ^{13}C and ^{2}H nuclei possess different orientations. Therefore, these interactions are particularly sensitive to different features of the chains' orientation distribution. In addition, natural-abundance ^{13}C experiments open opportunities for a wide range of applications not limited by the need for often expensive or inconvenient isotropic enrichment in laboratory sample preparations. Indeed, all samples discussed below originate from industrial process lines, and the films investigated are an order-of-magnitude thinner than many deuterated samples prepared in the laboratory.[9] Practical ramifications are obvious, as this permits detailed investigation of molecular orientation as a function of sample process history, shedding new insight on the relevance of process variables to macroscopic material performance.

Conventional 1D ^{13}C NMR spectra with cross-polarization from protons to ^{13}C nuclei, shown in Figure 1, of a biaxially drawn industrial PET film reveal pronounced sensitivity to the orientation of the sample with respect to the applied magnetic field. In particular, the analysis of the spectrum of Figure 1b, with $\mathbf{B}_0$ perpendicular to the

0024-9297/93/2226-2282$04.00/0

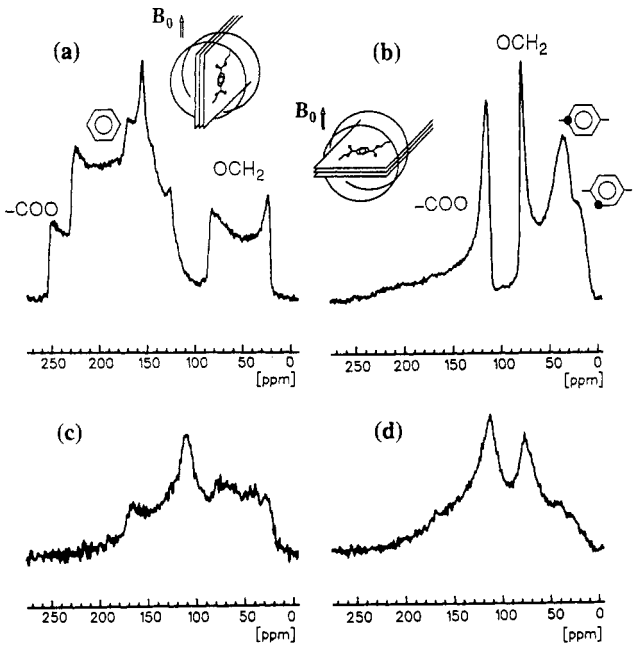

Figure 1. 1D static ^{13}C NMR spectra for a biaxially drawn, 12-μm PET film with its machine direction (MD) parallel to the receiver coil axis. Spectra a and b were obtained after cross-polarization and a Hahn spin echo; they correspond to sample orientations in which either (a) the transverse direction (TD) or (b) the normal direction (ND) was parallel to the applied magnetic field $\mathbf{B}_0$. Spectra c and d were obtained with ^{13}C single-pulse excitation using a 1-s recycle delay, which selects for the most highly mobile segments. The orientations of (c) and (a) are the same, as are (d) and (b). Little orientation dependence is observed for the mobile components.

film plane, shows[10] that the planes of the phenylene rings and carboxyl groups are essentially parallel to the planes of the sheets: for each of these groups, the spectral intensity is concentrated at the upfield principal value of the spectrum, which means that the principal axis perpendicular to the planes of the molecular structures is parallel to $\mathbf{B}_0$. However, a fraction of disordered segments is also present in the sample. This is proven by the essentially rotationally invariant spectra of the same material in Figure 1c,d, acquired with single-pulse excitation such that segments with short ^{13}C T_1 relaxation times, that is, high-frequency molecular motions, are selectively observed. The various spectra in Figure 1 show that the orientation distribution is relatively complicated and therefore difficult to quantify from these data. Actually, in one-dimensional spectra the frequency is measured only once, providing information equivalent to the specification of only one Euler angle of the segmental orientation (relative to some sample-fixed frame). In addition, resolution difficulties posed by overlapping signals often render of limited value spectra acquired with the $\mathbf{B}_0$ field displaced from the main ordering direction of the sample. Such spectra, however, are essential for a precise analysis of the orientation distribution function.[11] For PET, overlapping resonances from carboxyl and phenylene group carbons are especially troublesome, and as a consequence restrict the angular information achievable in one-dimensional NMR experiments.

Expansion of the information available from anisotropic NMR interactions into a second frequency dimension has been shown to be an effective means of enhancing the information content of solid-state NMR spectra. This has permitted sensitive measurements of orientational order in partially ordered solids[10,12,13] and of the orientations of NMR interaction tensors in single crystals.[14,15] Under conditions of magic-angle spinning (MAS), 2D NMR methods provide increased spectral resolution, though at the expense of angular precision. Nevertheless, 2D MAS NMR has yielded information on chain order in PET at a molecular level.[12] The technique to be employed in this paper, introduced by Henrichs[10] and recently extended by us,[13] is termed "Direction Exchange with Correlation for Orientation-Distribution Evaluation and Reconstruction" (DECODER). It measures and correlates NMR frequencies at two different sample orientations. Through this correlation, the spectra contain the equivalent of information on *two* Euler angles that describe the orientation of a given molecular segment. Many features of the orientation distribution are directly reflected in the intensity distribution of the two-dimensional spectrum, from which the width of the orientation distribution of certain axes can immediately be read. In fact, as pointed out in ref 13, close analogies exist between this 2D NMR experiment and wide-angle X-ray scattering techniques, such as pole-figure analysis. In its experimental and spectral features, the 2D DECODER experiment possesses close relations to multidimensional exchange NMR[16] methods that have witnessed powerful application to the study of dynamical phenomena,[17-20] notably in polymeric systems.[19,20]

The discussion of the two-dimensional DECODER patterns will rely heavily on the important case of axially symmetric chemical-shift tensors (asymmetry parameter $\eta = 0$), as described previously.[13] For many purposes this represents a good approximation up to η values of about 0.3, and many of the results derived for vanishing η can be qualitatively applied also to analyze spectra for large η values. The simulations will be extended to arbitrary η, considering isotropic, transverse isotropic, and biaxial samples. Typical spectral shapes for uniaxial and biaxial orientation distributions in drawn PET fibers and thin PET films prepared under different processing conditions will be presented. Thus, the study of orientation in PET films performed by Henrichs[10] is considerably expanded through use of various sample configurations, as we explain the direct relation between the features of the orientation distribution and the distribution of spectral intensity. It will be pointed out how the orientational distribution can in part be directly reconstructed from the spectral intensity or be read from the spectra in a semiquantitative fashion and how, in combination with spectral simulations, specific quantitative details on PET structure and orientation are provided. Thus, the full potential of the DECODER technique is demonstrated.

II. Theory

To facilitate discussion of specific DECODER NMR spectra of PET, we present some theoretical background for the analysis of such lineshapes. We first consider a few general aspects of exchange NMR, including 2D DECODER spectra from isotropic samples. This is followed by definitions of the angles and coordinate systems required for the orientation analysis and a discussion of orientation distribution functions and their moments. After a short discussion of DECODER lineshapes, it will be shown how relevant one-dimensional cross-sections through the full orientation distribution can be obtained directly from DECODER spectra.

Exchange NMR. Detailed information on molecular orientations can be obtained from solid-state NMR methods because the NMR frequencies depend on the orientation of a given molecular unit relative to the external

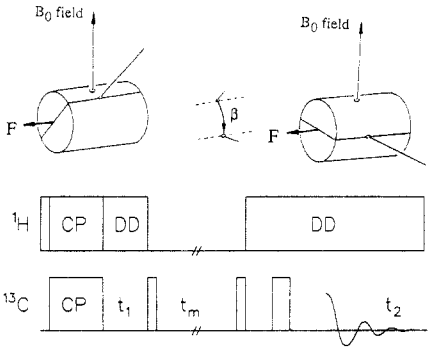

Figure 2. Schematic representation of the 2D DECODER exchange NMR experiment with sample reorientation. Due to the rotation of the sample during the mixing time, the angle-dependent NMR frequency is different in the evolution (t_1) and detection (t_2) periods. For simplicity, the sample orientation is indicated by an axis perpendicular to the flip axis **F**. Note that this need not be the order axis $\mathbf{Z}_D$ of the sample for the molecular orientations and frequencies to be altered by the sample rotation. Actually, they change even when the shapes of the 1D spectra do not change upon rotation, e.g., when the sample director $\mathbf{Z}_D$ is along **F**. During the repetition delay between successive scans, the sample is rotated back to its initial orientation.

magnetic field $\mathbf{B}_0$:[21,22]

$$\omega_{aniso}(\theta,\phi) = {}^1/_2\delta\{3\cos^2\theta - 1 - \eta\sin^2\theta\cos(2\phi)\} \quad (1)$$

where (θ,ϕ) denotes the orientation of the $\mathbf{B}_0$ field in the principal axes system of the anisotropic NMR interaction under consideration. In the context of this paper, we will be concerned with the anisotropic chemical shift interaction. The parameters δ and η, $0 \le \eta \le 1$, are specific for every site in the molecule. They are related to the principal values (σ_x, σ_y, σ_z) of the chemical shift tensor, and the corresponding frequencies $\omega_\alpha = \sigma_\alpha\omega_0$, according to

$$\delta = \omega_z - \omega_{iso} \quad (2)$$

$$\eta = (\omega_y - \omega_x)/\delta \quad (3)$$

with the isotropic chemical shift $\sigma_{iso} = \omega_{iso}/\omega_0$. A common convention[21,22] is used to define the order of the principal values: $|\omega_x| < |\omega_y| < |\omega_z|$. This choice is convenient for general theoretical considerations; in particular, for $\eta = 0$ it always identifies the unique principal axis as the z axis, irrespective of the sign of δ.

A schematic representation of 2D DECODER NMR as applied to ^{13}C is shown in Figure 2. It represents a two-dimensional (2D) exchange NMR experiment: reorientations during a mixing time t_m can be detected by measuring the angle-dependent NMR frequencies before and after t_m. Intensity $S(\omega_1,\omega_2)$ in the spectrum represents the probability of finding a molecular segment with a frequency ω_1 before t_m and with ω_2 afterward. In the absence of reorientation during t_m, no frequency change occurs, so that the spectral intensity is confined to the line $\omega_1 = \omega_2$, the diagonal in the frequency plane. Reorientations by one well-defined jump angle for an isotropic ("powder") sample generate 2D spectra with elliptical patterns, which depend on the reorientation angle β as shown in Figure 3.

In the DECODER experiment applied and analyzed in this paper, a rigid sample is reoriented, macroscopically and as a whole, during the mixing time. In practice, this involves rotation of the otherwise static sample through a discrete angle β during t_m, synchronized as shown in Figure 2 with the radiofrequency (rf) pulses that initiate and terminate the precession of the spins within the sample. After cross polarization, the spins precess for a time t_1 (evolution time) while the sample resides at some

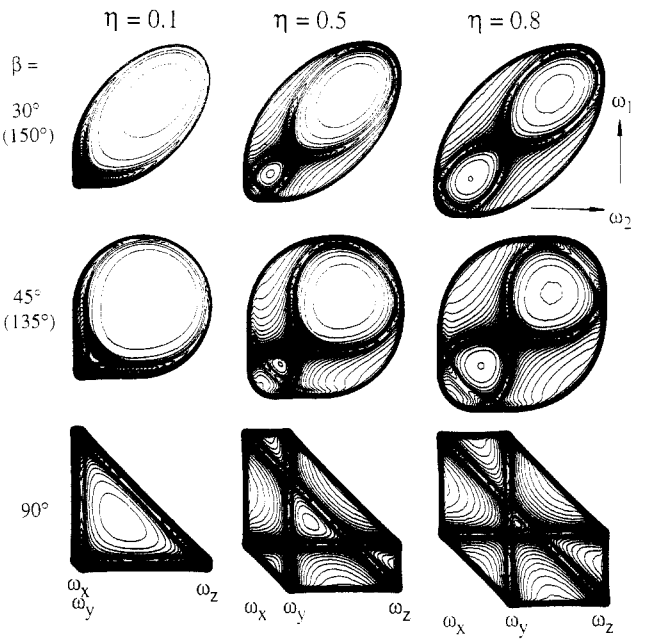

Figure 3. Simulated 2D exchange NMR spectra for isotropic samples (single site), subjected to different flip angles β, illustrating in particular the effects of nonzero asymmetry parameter η.

orientation (β_1,α_1) relative to $\mathbf{B}_0$ field. One component of the magnetization is then stored along the z axis by a 90° pulse prior to the sample flip, with another 90° pulse returning the amplitude-modulated magnetization into the transverse plane. Signal detection occurs during time t_2 while the sample resides at a new orientation (β_2,α_2) relative to $\mathbf{B}_0$. The sample is reoriented back to its original position during the repetition delay to permit extended signal averaging.

Powder Spectra. Before discussing partially ordered samples, we summarize some important general features of 2D exchange powder spectra that are helpful in the analysis to follow. First, the 2D powder spectra are broadened inhomogeneously in both dimensions, but never fill the full square determined by the anisotropy in ω_1 and ω_2. This is seen most clearly in Figure 3. Apart from the obvious dependence on η, a sample-flip powder spectrum can only depend on the single angle β between the two $\mathbf{B}_0$ orientations in any sample-fixed frame; the isotropy of the sample dictates that the spectrum must be invariant under changes of any other angle. The most marked spectral features are elliptical patterns, with the half-axes a and b of each ellipse related to the flip angle β according to

$$|\tan\beta| = b/a \quad (4)$$

Other spectral features are straight ridges parallel to the spectral axes, with the "90° ridges"[17,18] as well-known examples. The elliptical patterns and 90° ridges are easily derived for axially symmetric NMR interactions ($\eta = 0$).[17,18] In this case, it can in fact be shown that equivalent exchange spectra are produced under the separate conditions of molecular motions and macroscopic sample reorientation.[13] For $\eta \neq 0$, the 2D powder spectra obtained in the two experiments are definitely different. The molecular reorientation must be specified in terms of three angles, connecting the principal axes system (PAS) orientations before and after the reorientation.[19] This leads to exchange figures that trace out higher-order curves. In contrast to this, the DECODER powder spectrum depends only on the single angle β. Thus, even for $\eta \neq 0$, ellipses are the dominant features in the powder spectra, as seen

clearly in Figure 3. The three ellipses observed here degenerate into a single one as η approaches zero.

For $\eta \neq 0$, ellipses are observed threefold in powder spectra and display jump-angle dependences analogous to that when $\eta = 0$. The smallest ellipse touches the frequency positions ω_x and ω_y in both dimensions, the largest one ω_x and ω_z, and the intermediate one ω_y and ω_z. However, in contrast to the case of $\eta = 0$, along the outer limits of the spectral intensity there are no ridges, but only edges. The elliptical features turn into ridges only in the interior of the 2D powder pattern (i.e., where they do not constitute part of the limits of the intensity in the 2D plane). Concerning the extension of the patterns in the frequency plane, note in particular that for $\beta \neq 0$ and $\eta \neq 0$, the corners (ω_x,ω_x) and (ω_z,ω_z) are not accessible. (ω_ξ,ω_ξ) would correspond to molecular orientations with $\mathbf{B}_0$ along the ξ axis during both the evolution and detection periods. This is, however, impossible since the sample is rotated around an axis perpendicular to $\mathbf{B}_0$; consequently, the two field orientations are separated by the angle β in the principal axes system. Only for $\eta = 0$, where all directions in the x–y plane of the PAS exhibit the same frequency, can the frequency remain unchanged.

The features of the 2D powder spectrum for a given flip angle β are also relevant in the analysis of spectra from oriented samples measured with the same β. The powder spectrum contains contributions from all possible orientations. Therefore, its boundaries represent the outermost limits for the 2D spectrum of any partially ordered sample. As will be seen below, in the intensity distribution of many spectra the location of the elliptical ridges plays an important role. In addition, the decrease of overlap in 2D DECODER spectra can be exploited to determine refined values of the principal values of the various shift tensors.[23]

Angles, Coordinate Systems, and Orientation Distributions. To describe the rather complex order phenomena in the PET samples, four different frames of references are relevant. They are displayed in Figure 4 together with the Euler angles through which they are related.

(*i*) *Laboratory frame* (*LF*): The direction of $\mathbf{B}_0$ defines the $\mathbf{Z}_L$ axis in the laboratory system.

(*ii*) *Sample-fixed director frame* (*DF*): The primary sample order direction is usually denoted as the sample director $\mathbf{Z}_D$, with accompanying orthogonal axes $\mathbf{X}_D$ and $\mathbf{Y}_D$. (β_1,α_1) are the polar coordinates of the $\mathbf{B}_0$ field in the sample-fixed director frame during the evolution time, and (β_2,α_2) are those of $\mathbf{B}_0$ during the detection period. Note that $\beta = \beta_2 - \beta_1$ only if the sample director $\mathbf{Z}_D$ is perpendicular to the rotation axis. For instance, if $\mathbf{Z}_D$ is along the flip axis, one has $\beta = \alpha_2 - \alpha_1$.

The rotation or flip axis, $\mathbf{F}$, is fixed in both the laboratory and the sample frames. The angle Γ, used in conjunction with the reconstruction procedure below, distinguishes sample-fixed directions in the "field plane", which is the plane containing all axes perpendicular to $\mathbf{F}$.

(*iii*) *Molecular frame* (*MF*): The molecular chain axis is usually chosen as the $\mathbf{Z}_M$ axis. (Ψ_M,Θ_M,Φ_M) are the Euler angles specifying the relative orientation of the molecular frame MF and the director frame DF. They are generally more structurally meaningful for specifying the orientation distribution than are (Ψ,Θ,Φ), the Euler angles of the relative orientation of PAS and DF, though (Ψ,Θ,Φ) are more directly connected to the measured frequencies.[13]

(*iv*) *Principal axes system* (*PAS*): The nuclear interaction tensor is diagonal in the PAS; it is fixed with respect to the molecular segment, often reflecting its local symmetries. For instance, for the planar phenylene rings and carboxyl groups, the principal axis corresponding to the upfield principal value points along the normal of the plane. $(\alpha_P,\beta_P,\gamma_P)$ are the Euler angles specifying the relative orientation of PAS and MF. Angles β_P and α_P are fixed by the tensor orientation in the molecular structure, being the polar coordinates of the molecular axis $\mathbf{Z}_M$ in the PAS. γ_P and Ψ_M, both involving rotations around the $\mathbf{Z}_M$ axis, have the same effect in the transformation PAS → MF → DF, so γ_P can be set to zero without restricting the generality of the treatment. The $\mathbf{B}_0$ field ($\mathbf{Z}_L$) orientations in the PAS are specified by (ϑ_1,φ_1) and (ϑ_2,φ_2).

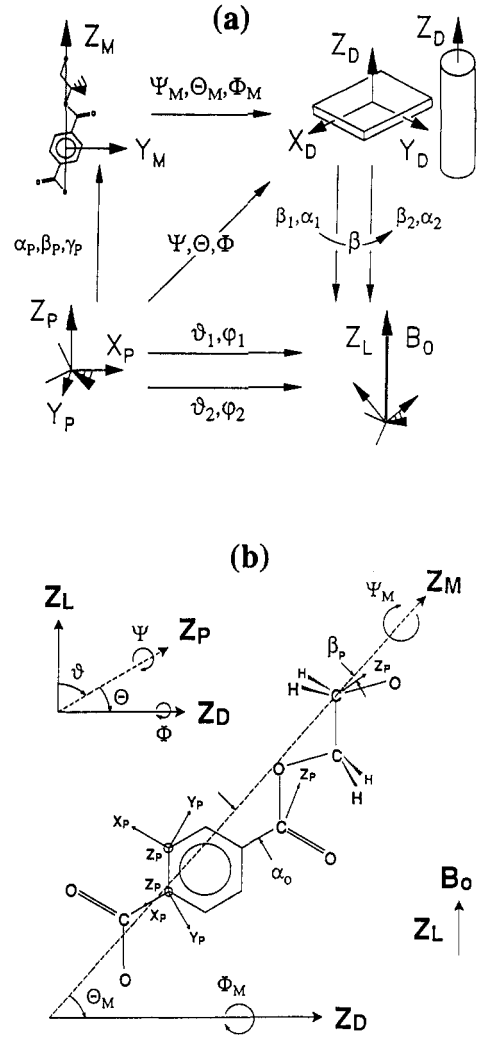

Figure 4. (a) Axes and coordinate systems relevant to the analysis of the DECODER experiment. (b) Definitions of angles describing chain, segmental, and chemical-shift tensor orientations in PET.

As is clear from eq 1, there is a direct correspondence between ω and $\cos^2\vartheta$ for $\eta = 0$, but no information on φ. The orientation of the $\mathbf{Z}_P$ principal axis for $\eta = 0$ in the sample-fixed frame can be specified in terms of the angles (Θ,Φ), which can be determined in many cases from the two frequency coordinates (ω_1,ω_2) in a 2D DECODER spectrum[13] and completely from $(\omega_1,\omega_2,\omega_3)$ in a 3D DECODER spectrum with a flip around two different axes of the sample. For $\eta \neq 0$, the orientation of every principal axes system in the sample-fixed frame must be specified. This requires specification of *three* angles, which can be established only by measuring the frequency at least *three* times, for instance in a 3D DECODER experiment. Maximum information could be extracted from a hypothetical 4D experiment with three different flip axes.

Several choices of the three angles required to specify the orientation distribution are possible. For most purposes, the Euler angles (Ψ_M,Θ_M,Φ_M) of the orientation of the molecular frame MF in the sample-fixed director frame DF are most appropriate. (Θ_M,Φ_M) are then the polar coordinates of a given molecular axis $\mathbf{Z}_M$ in the DF. The spectral features, however, reflect directly the distribution of (Ψ,Θ,Φ), the orientation of the PAS in the DF. Thus, for analyzing the distribution of chain axes in terms of Θ_M by means of the DECODER experiment, it is convenient if $\eta = 0$ and $\mathbf{Z}_P = \mathbf{Z}_M$, so that $\Theta_M = \Theta$. This favorable case is approximately met for the OCH_2 and carboxyl sites in PET.

The orientation distribution in systems that exhibit "transverse isotropy"[12] can be characterized in terms of Θ_M alone, because the definition of transverse isotropy dictates that all Ψ_M and Φ_M are present with equal probability, and thus their role in the orientation distribution is fully specified. The condition for Φ_M is equivalent to macroscopic uniaxiality; i.e., the distribution of the molecules or chains with respect to the sample director $\mathbf{Z}_D$ is cylindrically symmetric. The microscopic condition for Ψ_M is usually met on the basis of fiber symmetry, or when $\eta = 0$. For the first case, it must be considered that the chain axes in the crystalline fraction have a definite orientation relative to the molecular structure. However, this does not specify the angle Ψ_M that describes the rotation of the molecules around the chain axis. Consequently, equal probabilities for all values of Ψ_M are to be expected for a set of parallel chain axes $\mathbf{Z}_M$. In the case of $\eta = 0$, with the molecular axis $\mathbf{Z}_M$ chosen along the unique principal axis $\mathbf{Z}_D$, different values of Ψ_M are not distinguishable, because a rotation around $\mathbf{Z}_D$ leaves the frequency, and therefore also the spectrum, invariant. With a uniaxial distribution of chain axes, the two conditions for transverse isotropy are fulfilled.

Characterization of Biaxial Samples. While for uniaxial samples with transverse isotropy the orientation distribution can be specified in terms of a single angle, such as Θ or Θ_M, in the case of macroscopic and microscopic biaxiality three angles, such as Θ, Φ, and Ψ, must be taken into account in the analysis. In drawn polymers the relevant distribution functions have a periodicity of 180°. The simplest form for this is

$$P(\Psi,\Theta,\Phi) = \exp(-\sin^2\Theta/(2\Theta_\sigma^2))\exp(-\sin^2\Phi/(2\Phi_\sigma^2)) \times \exp(-\sin^2\Psi/(2\Psi_\sigma^2)) \quad (5)$$

In the denominators of the exponents, we employ, for instance, $2\Theta_\sigma^2$ instead of the more commonly used $2\sin^2\Theta_\sigma$,[7] because with $2\Theta_\sigma^2$, we can also parameterize wide distributions, while the range of $\sin^2\Theta_\sigma$ is restricted. For small Θ_σ, the expressions are similar. Below, we will characterize the distributions in terms of their full-widths-at-half-maximum (fwhm), denoted by $\Delta\Psi$, $\Delta\Theta$, and $\Delta\Phi$. Since the fwhm's become meaningless for very wide distributions, consistently but more generally we define $\Delta\Psi = 2(2\ln 2)^{1/2}\Psi_\sigma$, $\Delta\Theta = 2.355\Theta_\sigma$, and $\Delta\Phi = 2.355\Phi_\sigma$. This factor of $2(2\ln 2)^{1/2} = 2.355$ must be taken into account in comparing widths of angular distributions and their error margins in various investigations of orientational order in drawn polymers.[9,11]

Simulated spectra in Figure 5 show how biaxiality can be directly detected in 2D DECODER spectra. A flip angle of $\beta = 40°$ was chosen for a configuration with the primary sample director $\mathbf{Z}_D$ along the flip axis $\mathbf{F}$, $\Theta = 90°$, and $\eta = 0.28$. Figure 5a is based on cylindrical symmetry in Φ, while Figures 5b and 5c are based on biaxial distributions

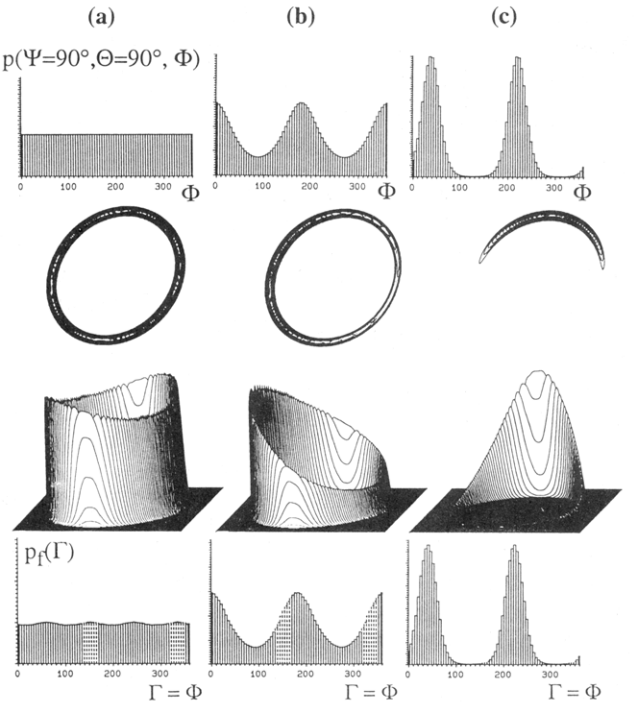

Figure 5. Detection of biaxiality in (simulated) 2D DECODER spectra, with $\beta = 40°$ and the director axis $\mathbf{Z}_D$ parallel to the flip axis $\mathbf{F}$. The asymmetry parameter was chosen to be $\eta = 0.28$, as found for the OCH_2 groups in PET. The $\mathbf{Z}_P$ axes are perpendicular to the sample director $\mathbf{Z}_M$ (i.e., $\Theta = 90°$), and $\Psi = 90°$ as for the OCH_2 groups in PET.[36] The top row displays the distributions in Φ, the middle rows the corresponding DECODER spectra with contour and stacked plots, and the bottom row the distributions of $\mathbf{Z}_P$ axes in the field plane reconstructed from the spectra. It is apparent that the reconstruction reproduces the original distributions faithfully. For the dashed range between 135 and 170°, the reconstruction is not unique.[13] For the reconstructions, the flip angle was intentionally misset to 42° (instead of 40°); the only visible effect this produces is the ripple on the reconstructed distribution in (a). The distributions were chosen to be Gaussians according to eq 5: (a) infinite half-width $\Delta\Phi$ (uniaxial sample); (b) half-width $\Delta\Phi = 80°$; one round trip along the ellipse corresponds to a 180° change in Φ; (c) half-width $\Delta\Phi = 40°$.

with $\Delta\Phi = 80°$ and $\Delta\Phi = 40°$, respectively. Points on the nearly circular spectral pattern separated by an angle 2Γ belong to orientations differing by $\Phi = \Gamma$.[13] Therefore, the width of the distribution in Φ can be determined directly from the length of the arc, as is discussed immediately below.

For a given problem, such as characterization of biaxiality or exact measurement of the width of the orientation distribution around a given or presumed Θ_0, special choices of sample orientations are often most appropriate. For interpreting the 2D DECODER spectra, it is helpful to recall that the 1D spectra for the orientations in the evolution and the detection period represent the projections of the 2D spectrum onto the spectral axes. This fact, together with the restrictions indicated by the corresponding 2D powder pattern, and possibly a simple analysis in the sample-fixed frame, makes it possible to predict most features of a 2D spectrum and to some extent even to tailor them to a particular need, such as eliminating overlap between different components in the spectra. Table I lists sample configurations and flip angles most suitable for elucidating certain features of the distribution of orientations and for reducing spectral overlap.

Order Parameters and Moments. As an alternative to analysis directly in terms of the distribution function $P(\Psi_M,\Theta_M,\Phi_M)$, order parameters can be calculated,[10,25-27]

Table I
Survey of Sample Orientations and Flip Angles Best Suited for Elucidating Spectral Features Associated with the Accompanying Distribution Functions

sample configuration	flip angle	features
uniaxial samples		
order axis ∥ **F**	$\beta = 90°$	minimal overlap, simple sample preparation
order axis ⊥ **F**	$\beta \approx 45°$	maximum angular resolution
order axis ∥ $\mathbf{B}_0$ during t_1 or t_2	(any β)	little overlap
$\beta_1 = \beta_2$ (angles between $\mathbf{Z}_D$ and $\mathbf{B}_0$) $\alpha_1 = \alpha_2 + 180°$	$2\beta_i = \beta \approx 45°$	symmetric spectrum, wide range around $\theta = 0°$ is reconstructible
$\beta_2 = 180° - \beta_1$ $\alpha_1 = \alpha_2$	$\lvert\beta_2 - \beta_1\rvert = \beta \approx 45°$	symmetric spectrum, wide range around $\theta = 90°$ is reconstructible
biaxial samples:		
MD or TD ∥ **F** (out-of-plane configuration)	$\beta \approx 45°$	out-of-plane distributions, simple sample preparation
ND ∥ **F** (MD and TD ⊥ **F**) (in-plane configuration)	$\beta \approx 45°$	in-plane distribution

from the distribution according to

$$\langle D^L_{MN}(\Psi_M,\Theta_M,\Phi_M)\rangle = (8\pi^2)^{-1}\int\int\int d\Psi_M\, d\cos\Theta_M \times d\Phi_M\, P(\Psi_M,\Theta_M,\Phi_M)\, D^L_{MN}(\Psi_M,\Theta_M,\Phi_M) \quad (6)$$

where the $D^L_{MN}(\Psi_M,\Theta_M,\Phi_M)$ are the Wigner rotation matrix elements, as given in refs 28 and 29. Averages of the type described by eq 6 are measured directly by several techniques. The order parameters are closely related to the moments P_{LMN} of the distribution, which are the expansion coefficients in

$$P(\Psi_M,\Theta_M,\Phi_M) = \sum_L\sum_M\sum_N P_{LMN} D^L_{MN}(\Psi_M,\Theta_M,\Phi_M) \quad (7)$$

By inserting eq 7 into eq 6, the following relation between order parameters and moments is obtained:

$$P_{LMN} = (2L+1)\langle D^L_{MN}(\Psi_M,\Theta_M,\Phi_M)\rangle \quad (8)$$

We employ the order parameters, as they correspond to averages commonly discussed, such as

$$\langle D^1_{00}\rangle = 1, \quad \langle D^2_{00}\rangle = {}^1/_2\langle 3\cos^2\Theta_M - 1\rangle$$

$$\langle D^4_{00}\rangle = {}^1/_8\langle 35\cos^4\Theta_M - 30\cos^2\Theta_M + 3\rangle \quad (9)$$

The calculation of the order parameters for the distributions obtained from the DECODER spectra is useful for a comparison with the results from other methods. However, in making such a comparison it should be taken into account that the moments depend on the sample coordinate system of reference. The transformation can be effected on the basis of the transformation properties of the $D^L_{MN}(\Psi_M,\Theta_M,\Phi_M)$, for which an example is given below.

The orientational moments are suitable for a relatively simple description of the orientation distribution, in particular for uniaxial systems, where all order parameters vanish except for $P_L = \langle D^L_{00}(\Psi_M,\Theta_M,\Phi_M)\rangle$,[25-28] so that only the Legendre polynomials $P_L(\cos\Theta_M) = D^L_{00}(\Psi_M,\Theta_M,\Phi_M)$ are relevant. In this context, contrary to the more general nomenclature described above, the P_L are normally referred to as the moments of the distribution.

The significance of the order parameters of moments with nonvanishing N and M that appear for biaxial systems is less common knowledge, so that characterization in terms of the widths of product functions (as mainly employed in this paper) may be easier to visualize. For materials with microscopic and macroscopic orthorhombic symmetry,[10,25,27] all moments with odd L, M, or N vanish, such that the number of moments to be actually calculated is significantly reduced. In the interpretation of the values given below, it should also be noted that not all order parameters can reach a maximum value of 1.0; $\langle D^2_{20}\rangle$ and $\langle D^2_{02}\rangle$, for instance, have a maximum of $(3/8)^{1/2} = 0.6123$, as derived immediately from the D^2_{02} and D^2_{20} functions,[28,29]

$$\langle D^2_{20}\rangle = (3/8)^{1/2}\langle \sin^2\Theta_M \cos(2\Psi_M)\rangle$$

$$\langle D^2_{02}\rangle = (3/8)^{1/2}\langle \sin^2\Theta_M \cos(2\Theta_M)\rangle \quad (10)$$

while $\langle D^2_{22}\rangle$ has a maximum of 0.5 for distributions symmetric with respect to $\Theta = 90°$.

2D DECODER Lineshapes. The width of the distribution of orientations is directly reflected in the width of the distribution of intensity in the DECODER spectrum. This spread is naturally confined to and can be compared with the limits of the powder spectrum for the given δ, η, and flip angle β. For $\eta = 0$, the spectral patterns are directly related to the distribution of $\mathbf{Z}_P$ axes in terms of Θ and Φ,[13] with certain reductions due to symmetry; the spectral intensity does not depend on Ψ. This helpful degeneracy is lifted if $\eta \neq 0$, such that the intensity spreads out as a function of Ψ and mixes with the effects of Θ and Φ. It would require at least a 3D DECODER experiment[10] to separate those effects in the general case. Still, if certain constraints on one of the variables are specified, the patterns in a 2D DECODER experiment are characteristic of the others. In addition, by a suitable choice of sample orientation and flip angle, different orientational properties can be emphasized. Space does not permit us to show and describe here the large variety of spectral patterns resulting for $\eta \neq 0$ upon variation of Ψ, Θ, and Φ; this topic is treated in some detail in ref 22. Overall, the shapes of the spectral patterns resemble those observed for $\eta = 0$ with the same flip geometry:[13] for instance, with $\mathbf{Z}_D$ parallel to **F** and $\beta = 45°$, circular patterns result predominantly, while straight lines mainly result for $\beta = 90°$. Examples of these features are found in the simulations of the experimental spectra shown below.

Direct Reconstruction of Orientational Distributions. For small η, the distribution of $\mathbf{Z}_P$ axes in the field plane (the plane perpendicular to the rotation axis **F**) can be reconstructed particularly conveniently and reliably from experimental data. The location of the spectral intensity corresponding to the field plane is the elliptical ridge in the 2D powder pattern for $\eta = 0.1$ in Figure 3. It exhibits high intensity (only at the expense of resolution in the out-of-field-plane coordinate, which is of little interest here). In addition, for $\Theta \approx 45°$ the intensity distribution along the ridge is not distorted by the angle-dependent frequency, so that the angular resolution along the ridge is constant. This is an advantage compared to 1D NMR spectra, where the angular resolution is extremely low at the edges of the spectral range. One-dimensional spectra also have the disadvantage of representing only a projection of the angular distribution, so that different portions of the distribution overlap, often inextricably.

In the following, the angle Γ will denote the orientation in the field plane relative to some sample-fixed direction. The relation between Γ and the angles Θ and Φ depends on the sample frame of reference: for the in-plane configuration, we have Γ = Φ (at Θ = 90°); for the out-of-plane configuration, Γ = Θ (at a certain Φ). Thus, using these different sample orientations the distribution $p_f(\Gamma)$ along the elliptical ridge scans orthogonal slices, along Θ and Φ, through the distribution $P(\Theta,\Phi)$. Over a Γ range of about 140°, the relation between Γ and the location along the elliptical ridge is unique. The restriction to less than the full 180° range is a consequence of overlap with signal from other orientations that can occur near the (ω_y,ω_y) singularity.[13] This limitation can be neglected, however, if the distribution of $\mathbf{Z}_P$ axes is known to be concentrated around the field plane; under these circumstances, $p_f(\Gamma)$ can be reconstructed over the full Γ range of 180°. The power of the reconstruction of $p_f(\Gamma)$ will become apparent in the application of this very direct method of data analysis to the experimental spectra below. The procedure requires as parameters only the chemical-shift principal values and the flip angle β, which can be determined with high accuracy.

Reconstruction of Chain-Axis Distributions. The distribution of chain axes can be determined most directly if the $\mathbf{Z}_P$ axis is parallel to the chain axis ($\beta_P = 0$). In uniaxial systems, actually for any known β_P, the desired distribution $p_M(\Theta_M)$ of $\mathbf{Z}_M$ axes can be obtained from the distribution $p(\Theta) = u(\Theta)/\sin\Theta$ of $\mathbf{Z}_P$ axes, as measured in the DECODER experiment. This transformation, which does not involve any assumptions on the shape of the distribution functions, is not trivial: it resembles a deconvolution, removing the broadening introduced by the distribution (in Ψ) of the $\mathbf{Z}_P$ axes around the chain axis $\mathbf{Z}_M$. The algorithm applied here is based on the simple relationships[8] between the moments of the distributions $p(\Theta)$ and $p_M(\Theta_M)$

$$\langle P_L(\cos\Theta)\rangle = \langle P_L(\cos\Theta_M)\rangle P_L(\cos\beta_P) \qquad (11)$$

which in turn can be derived from the spherical harmonics addition theorem.[26,28] From the measured $p(\Theta)$, we determine the moments $\langle P_L(\cos\Theta)\rangle$, and then the $\langle P_L(\cos\Theta_M)\rangle$ according to eq 11; from these, $p_M(\Theta_M)$ is generated according to the superposition formula eq 7, which simplifies to

$$p_M(\Theta_M) = \sum_L (2L+1)\langle P_L(\cos\Theta_M)\rangle P_L(\cos\Theta_M) \qquad (12)$$

III. Experimental Section

The DECODER experiments were performed on industrial PET (Mylar) film samples provided by E. I. du Pont de Nemours S. A., Luxembourg. In addition to biaxially drawn films, uniaxial films from upstream stages of the production process were also examined. Commercial biaxial films were nominally 12 μm thick and taken from various points in an industrial process line. Film densities were measured to be 1.396 g/cm^3, corresponding to a crystallinity of 40 ± 10%.[4,30,31] The crystallites are sufficiently small to render the films transparent. The glass transition temperatures of the samples were measured to be 340 K. The films were handled above their T_g's during the production process, which involved initial longitudinal stretching to produce uniaxial orientational order, followed by transverse stretching to impart biaxiality. The direction of longitudinal stretching is commonly referred to as the machine direction MD, the transverse direction is denoted as TD, and the normal of the film plane is the normal direction ND. All biaxial films were heat-set above 470 K under longitudinal and transverse tension before being cooled to room temperature. Uniaxial films, 65 μm thick, were acquired before the transverse stretching stage. For purposes of comparison, an isotropic bulk PET sample was prepared by melting a separate portion of biaxial film material.

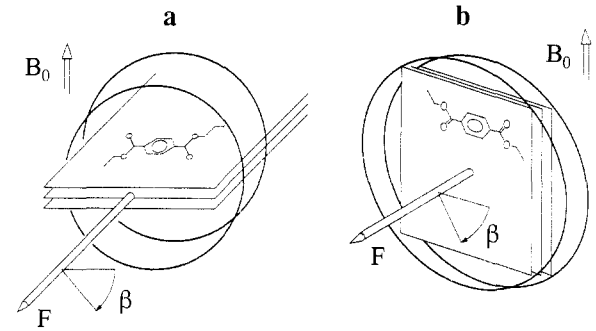

Figure 6. Schematic diagram depicting sample orientations in which the plane of the film is positioned (a) parallel with or (b) normal to the axis of the receiver coil, which is also the flip axis **F**. With respect to the applied $\mathbf{B}_0$ field, these orientations are referred to as out-of-plane or in-plane configurations, respectively.

To meet sample geometry constraints imposed by the NMR experiment, the films were assembled in a stacked arrangement to fit the 7.5-mm-diameter coil of the NMR probehead. Paying careful attention to the preservation of film orientation, the films were cut and collected into the two configurations shown in Figure 6, one with the sample rotation axis **F** parallel to the plane of the film (Figure 6a), and the second with the axis **F** perpendicular to the film plane (Figure 6b). We refer to the two arrangements as out-of-plane and in-plane configurations, respectively, based on their relationship to the applied magnetic field $\mathbf{B}_0$. The uncertainty introduced by film misalignment is estimated to be less than ±2° for the out-of-plane configurations and less than ±5° for the in-plane arrangements. From analysis of numerous samples, it can be said with confidence that the distributions of orientations measured are true reflections of inherent anisotropic properties of the material and not artifacts arising from sample handling procedures.

Another NMR sample was prepared from a collection of PET fibers, Trevira (Hoechst Co., Frankfurt) with a fiber size of 5 tex (5 g/1000 m). These fibers were cut from a single PET filament and assembled into a 7-mm-diameter bundle, so that the fiber draw directions were parallel to the axis of sample rotation. The uncertainty introduced by fiber misalignment is estimated to be less than ±5°. For fibers and extruded or drawn samples, orientation of the draw axis along the coil is convenient both in terms of sample preparation and for subsequent analysis of the data. Compared to other NMR experiments for characterizing orientation,[12] sample preparation for the DECODER experiment is quite simple, since no stable continuous rotation of the sample is required as in MAS experiments.

All ^{13}C NMR spectra were acquired at room temperature on a Bruker MSL-300 spectrometer operating at a ^{13}C frequency of 75.47 MHz. A home-built ^{13}C–^{1}H double-resonance probehead was employed to rotate the sample about the coil axis, using a rack-and-pinion (cogged spindle and wheel) mechanism, driven by a stepping motor that was computer-controlled synchronously with the 2D pulse program. Pulse sequences employing cross-polarization from protons to naturally abundant ^{13}C were used with a Hahn echo prior to signal detection as shown in Figure 2. The 90° pulse length was 4 μs. Flip times were about 600 ms for a 90° sample flip. For ^{13}C in natural abundance, flip times up to 1 s usually do not present disadvantages, as ^{13}C spin diffusion is negligible on these time scales. However, signals are suppressed by these flip times if their ^{13}C T_1 relaxation times are shorter, which usually results from large-amplitude motions, e.g., methyl group rotation. Because the chemical-shift anisotropies are scaled down by such motions, angular resolution for these segments is typically poor and consequently of little utility. In most cases, time-domain data sets with 40 t_1 increments of 24 μs were measured, with 400 scans each and recycle delays of 5 s.

To check the performance of the flip mechanism, a "quasistatic" ^{13}C DECODER experiment was performed, flipping the PET film sample by 40° and returning it to its initial orientation before signal detection. As this leaves all frequencies unchanged, a diagonal spectrum should result, as was indeed observed. This

Table II
Principal Values (±3 ppm) of the ^{13}C Chemical-Shift Tensors for the Different Carbon Sites in PET

segment	σ_x	σ_y	σ_z	δ	η
COO	113	126	252	88	0.15
OCH_2	87	76	22	−40	0.28
protonated phenyls	223	158	13	−118	0.55
unprotonated phenyls	228	146	31	−104	0.79

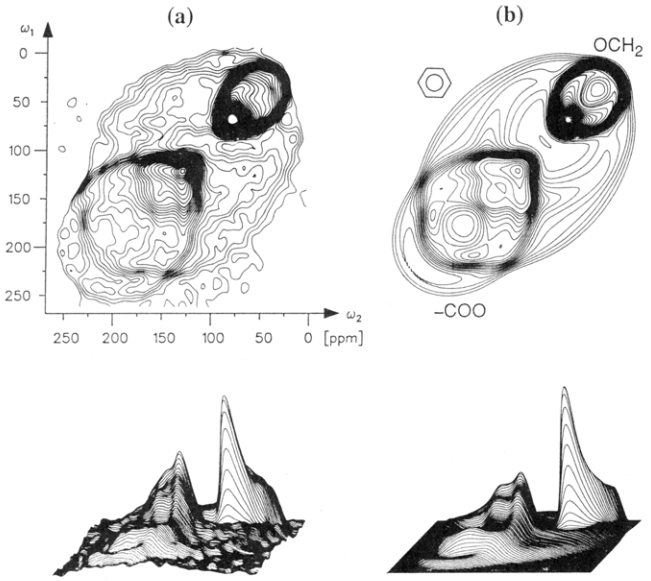

Figure 7. (a) 2D ^{13}C DECODER spectra (contour and stacked plots) for an isotropic bulk PET sample flipped through an angle $\beta = 40°$ during the mixing time. (b) Five-site simulation spectrum obtained using the principal values of the chemical-shift tensor for each segmental group shown in Table II. Contributions from the various segmental groups are identified. Note that the frequency patterns for the axially symmetric OCH_2 and carboxyl carbons are directed in opposite directions along the diagonal, reflecting opposite signs for the anisotropy parameter δ.

also proves that molecular dynamics, in particular possible phenylene ring flips, do not produce appreciable exchange intensity in the DECODER spectra of the PET films.

IV. Results and Discussion

Chemical-Shift Tensors in PET. For the analysis of the DECODER spectra, accurate knowledge of the chemical-shift tensors is required. Both the principal values of the tensors and the orientations of the principal axes in the corresponding molecular segment must be known, since these are the basis of the relation between the location of a signal in the spectrum and the actual orientation of the molecular segment in space. In the process of analyzing 1D spectra of the oriented films and of simulating the DECODER spectra, certain of these values which were known only with restricted accuracy could be refined to produce a single consistent set of principal values and axes to be used in all the simulations that follow below.

Table II lists the principal values of the chemical-shift tensors for the four chemically inequivalent carbon sites in PET. Previously reported values in the literature, obtained from 1D MAS and static spectra,[10,32] were used as starting points in the simulation analysis. These were refined on the basis of static 1D spectra of the annealed films, where reduced spectral overlap permits the range spanned by the anisotropies to be established with precision. The principal values were cross-checked with the 2D DECODER data in Figure 7 for isotropic bulk PET, exploiting the expanded frequency presentation. The error limits are ±3 ppm (2–6% of the full anisotropies). In the spectrum for the isotropic sample, the resonance patterns of the OCH_2 carbons (upper right-hand corner) and the carboxyl carbons (lower left) reflect shift tensors that do not deviate appreciably from axial symmetry, supported by comparison with the simulations in Figure 3. The frequency distribution for the phenylene carbons, on the other hand, manifests nonaxial behavior, with separate signal contributions from the protonated and unprotonated species being unresolved.

The tensor orientations of the aromatic carbons are well characterized and known to be essentially invariant in typical organic materials, with the upfield principal value ω_z corresponding to the axis normal to the ring and the downfield value ω_x to the C–H or the radial C–C bond direction.[33] Possible fast phenylene ring flips by ca. 180°[34,35] leave the chemical-shift tensors of the unprotonated carbons essentially invariant. For the protonated sites, ω_z is also nearly unchanged, and the ω_x and ω_y values are shifted by only 16 ppm.

The chemical-shift tensor orientation of the OCH_2CH_2O moieties has been measured in both PET and PEO by means of 2D separated-local field spectroscopy.[36] The data show that the PAS of the chemical-shift tensor exhibits the molecular segment's reflection symmetry with respect to the C–C–O plane, with the $\mathbf{Y}_P$ axis directed normal to that plane. The $\mathbf{Z}_P$ axis makes an angle of 20 ± 5° with the normal of the H–C–H plane and an angle of 15 ± 5° with the CH_2–O bond. This can be related to the chain axis $\mathbf{Z}_M$ by the chemical bonding structure and in particular the angle α_0 between the chain axis $\mathbf{Z}_M$ and the phenylene para axis, which lies along the bond connecting an unprotonated phenylene carbon and its neighboring carboxyl carbon (see Figure 4b). Taking into account the 4° deviation between the CH_2–O bond and the phenylene para axis according to the X-ray structure of PET,[4,5] $\mathbf{Z}_P$ of the methylenes makes an angle of about

$$\beta_P^{CH_2} = \alpha_0 + 4° - 15° \pm 5° = \alpha_0 - 9° \pm 5° \qquad (13)$$

with the chain axis $\mathbf{Z}_M$. (This calculation assumes a planar structure; with the 20° out-of-plane rotation of the methylene groups,[4,5] slightly larger $\beta_P^{CH_2}$ values result, e.g., increasing from 7° in the planar to 9° in the nonplanar structure.) Literature values for α_0 are 20°[4,5] and 24°,[9,12,37] below we determine values of $\alpha_0 = 18 \pm 4°$ and $\beta_P^{CH_2} = 8 \pm 5°$.

In the case of the carboxyl carbons, the upfield edge of the powder spectrum is known to correspond to the normal of the carboxyl plane. The principal axis corresponding to the downfield (252 ppm) edge of the carboxyl spectrum, $\mathbf{Z}_P$ according to the convention specified above, has previously been assumed to be approximately parallel to the C–C bond joining the rings and the carboxyl groups, with a deviation in the direction of the C–O single bond. This can be determined more precisely from the PET fiber spectrum shown below, which yields a deviation by 18 ± 5° of the $\mathbf{Z}_P$ from the fiber axis $\mathbf{Z}_M$.

PET Fibers. The simplest orientational properties can be expected for PET fibers, as their orientation distribution is uniaxial and can be characterized in terms of a one-dimensional distribution $p(\Theta_M)$. Figure 8a displays a spectrum with the chain axes perpendicular to the rotation axis $\mathbf{F}$ and a flip angle of $\beta = 42°$. As the chain axes are aligned parallel to the $\mathbf{B}_0$ field in the detection period, the signals of the different moieties are relatively well separated. Figure 8c portrays the distribution $p_f(\Gamma)$ reconstructed from the spectral intensity of the OCH_2 groups. This is the distribution of OCH_2 $\mathbf{Z}_P$ axes in the plane perpendicular to the flip axis; it would directly represent the searched-for distribution of chain axes $p_M(\Theta_M)$ if $\mathbf{Z}_P$

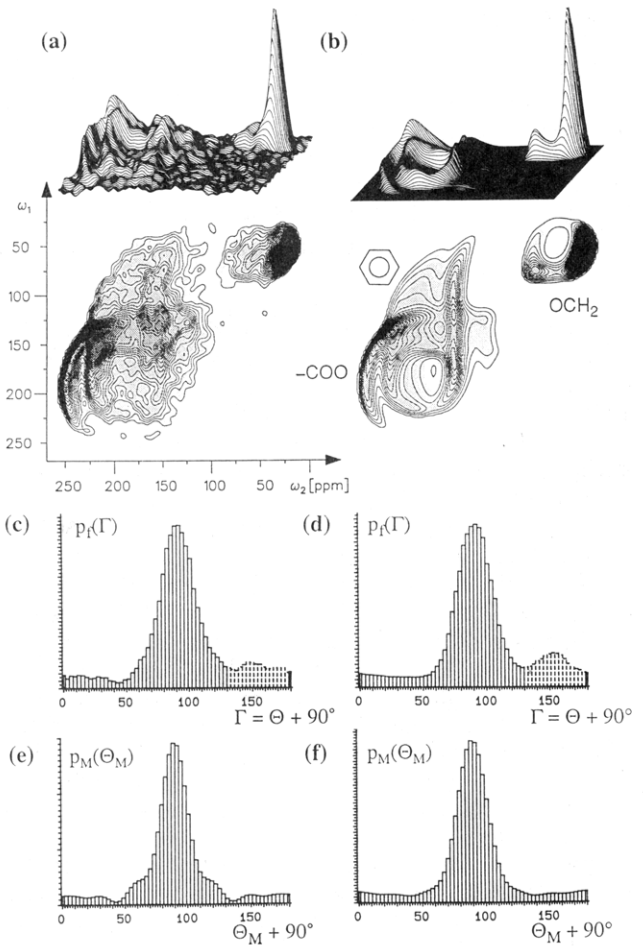

Figure 8. (a) 2D ^{13}C DECODER spectrum for a bundle of uniaxial PET fibers flipped through an angle $\beta = 42°$. The fibers were oriented perpendicular to the axis **F** of the receiver coil. In this spectrum, in addition to dominating signals from highly oriented material (fwhm $\Delta\Theta_M = 23 \pm 5°$), a contribution from a more disordered fraction of the sample (fwhm $\Delta\Theta_M = 135 \pm 45°$) is clearly detected, particularly in the OCH_2 pattern. (b) Simulated spectrum for a uniaxial sample with the five carbon sites in PET. (c) Distribution of $\mathbf{Z}_P$ axes reconstructed from the OCH_2 pattern of the experimental spectrum in (a); the fwhm is 30°. (d) Distribution of $\mathbf{Z}_P$ axes reconstructed from the OCH_2 pattern of the theoretical spectrum in (b), with a fwhm of 30°. (e) Distribution of chain axes obtained from the distribution in (d) (excluding the dashed range), exhibiting a fwhm of 24°. (f) Same as (e) for the distribution in (f), proving the reliability of the transformation: the narrow part of the distribution exhibits a fwhm of 25°, from a spectrum simulated on the basis of a distribution with a fwhm of 23°. In all of these angular distributions, the disordered component is apparent as a nearly orientation-independent background.

were parallel to $\mathbf{Z}_M$. Deviations of $\mathbf{Z}_P$ from $\mathbf{Z}_M$ broaden the distribution $p(\Theta)$ of $\mathbf{Z}_P$ obtained in the DECODER experiment as compared to $p_M(\Theta)$. On the other hand, a distribution with a pair of peaks, at $\pm\beta_P$, will be observed if the fwhm of $p_M(\Theta_M)$ is smaller than the angle β_P between $\mathbf{Z}_P$ and $\mathbf{Z}_M$. Therefore, several conclusions can be drawn on the basis of the plot in Figure 8c: the fwhm of $p_M(\Theta_M)$ must be 30° or less; on the other hand, it must exceed 15° since the distribution exhibits only a single sharp peak; for the same reason, the angle β_P between $\mathbf{Z}_P$ and $\mathbf{Z}_M$ must be smaller than 15°. In addition to the OCH_2 and carboxyl signals of high intensity at the upfield and downfield ends of the spectral range, which derive from the highly ordered fraction of the sample, more spread-out intensity corresponding to these moieties is observed both in the 2D spectrum and in the angular distribution of Figure 8. This is a clear indication of a fraction of considerably more disordered segments. In the simulations, this disordered fraction was found to have a fwhm of about 135°: it certainly exceeds 90°, but is apparently also not completely isotropic. Here as below, the signal contribution for the disordered OCH_2 groups does not exhibit the distinctive elliptical ridge expected; this could be a consequence of some motional averaging of these disordered components.

The distribution shown in Figure 8c has been subject to the transformation from $p(\Theta)$ to $p_M(\Theta_M)$, as described in the theoretical section. The application of this algorithm to the distribution reconstructed from the theoretical spectrum demonstrates its good performance (Figure 8d,f). For the experimental distribution, on the basis of $\beta_P^{CH_2} \approx 8°$ derived from the α_0 determined below, the distribution $p_M(\Theta_M)$ shown in Figure 8e was obtained. It has a fwhm of 25°, which compares well with the half-width of 23° used for the highly ordered component in the full two-dimensional simulation. The procedure can also be employed to confirm the limits on $\beta_P^{CH_2}$: as expected according to the discussion above, for $\beta_P^{CH_2} > 13°$ unreasonable distributions are generated, with considerable negative contributions.

As mentioned above, the angle α_0 between the phenylene para axis and the chain axis $\mathbf{Z}_M$ represents an important structural detail in PET, for which various values are found in the literature. 2D DECODER NMR applied to the PET fibers oriented *along* the rotation axis **F** yields this angle with considerable precision. For the spectrum displayed in Figure 9a, a flip angle of $\beta = 90°$ was chosen, as it is particularly suitable for reducing the spectral overlap between the five different ^{13}C patterns. The relative orientation of the phenylene rings and the chain axis $\mathbf{Z}_M$ can be extracted with precision from the relative position of the three phenylene-carbon patterns. Note that the splitting between them can be established with much higher precision than the absolute position of any single spectral feature. From analysis of the end-point positions, or equivalently from 2D simulations, we found $\alpha_0 = 18 \pm 4°$ (cf. Figure 9b). To check the error limits, simulations for α_0 equal to 24° as used in the literature[9,12] or with $\alpha_0 = 12°$ are shown for comparison in Figure 9c,d, where the spectral patterns of the phenylene region clearly disagree with the experimental spectrum. Some broadening of the signals of the protonated phenylene sites is additionally observed in the experimental spectrum. Phenylene-ring flips by about 180° around the para axis occur in these fibers on the time scale of the sample-flipping;[38] this spreads the intensity of the protonated carbons between the corresponding signals that would be observed in the absence of molecular motion, as assumed in the simulation.

It should be pointed out that it is the distribution of the sample director $\mathbf{Z}_D$ in the PAS that is basically reflected in the spectra. Viewed from the PAS, $\mathbf{Z}_D$ is distributed, while $\mathbf{Z}_M$ has one fixed orientation. The desired relative orientation of chain axis $\mathbf{Z}_M$ and phenylene ring in the fibers is obtained on the basis of $\mathbf{Z}_M \approx \langle \mathbf{Z}_D \rangle$, which is valid because we have a narrow distribution. $\mathbf{Z}_M \neq \langle \mathbf{Z}_D \rangle$ can result if the chain axis runs in zigzag. The narrow distribution restricts the zigzag angle to 10° or less, in accordance with literature values.[4] The position of the short stripe for the carboxyl resonance, together with the shape of the carboxyl pattern in Figure 8, indicates an angle of $\beta_P = 18 \pm 7°$ between the carboxyl $\mathbf{Z}_P$ and the chain axis $\mathbf{Z}_M$.

The 2D ^{13}C DECODER experiments on drawn PET fibers thus provide both the orientation distribution and basic structural details associated with relative orientations

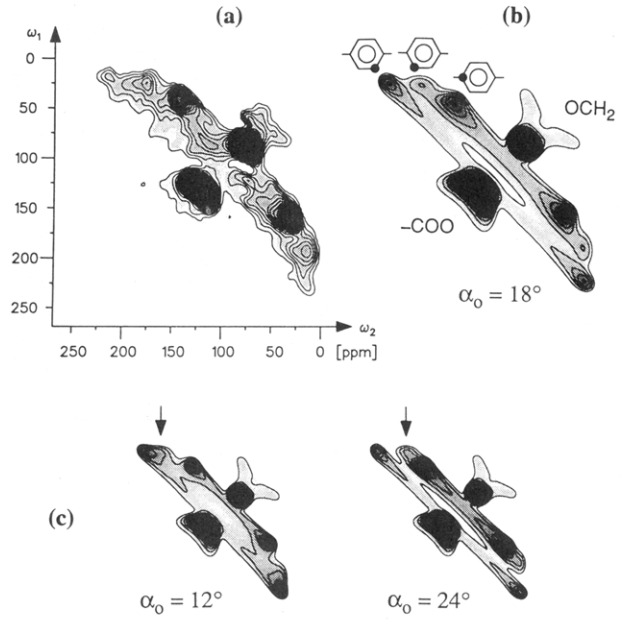

Figure 9. (a) 2D ^{13}C DECODER spectrum for a bundle of uniaxial PET fibers flipped through an angle $\beta = 90°$ during the mixing time. The fibers are oriented along the axis **F** of the receiver coil. (b) Five-site simulation for $\beta = 90°$ with the same distribution as in Figure 8, except for a reduction of the width of the distribution $\Delta\Theta_M$ to 20° (from 23°); this reflects the better alignment of the fibers in the coil for this sample configuration. For the simulation, a value of $\alpha_0 = 18°$ for the angle between chain axis $\mathbf{Z}_M$ and the phenylene ring para axis (Figure 4b) was used, which was found to best reproduce the features of the experimental spectrum. The intensity near the diagonal in the upper right-hand corner of the experimental spectrum arises from the disordered fraction of OCH_2 groups. Due to the strong signal concentration for the oriented component, most of the signal contributions from the 40% disordered material do not exceed the contour-level threshold of 5% of the maximum peak. Broadening of the patterns of the protonated aromatics is due to phenylene ring flips. (c) Two simulated spectra that employ α_0 values of 12 and 24°, showing the sensitivity of the phenylene carbon features to the angle α_0. The position of the pattern from the phenylene site closer in space to the OCH_2 units is particularly sensitive to α_0, as indicated by arrows above the plots.

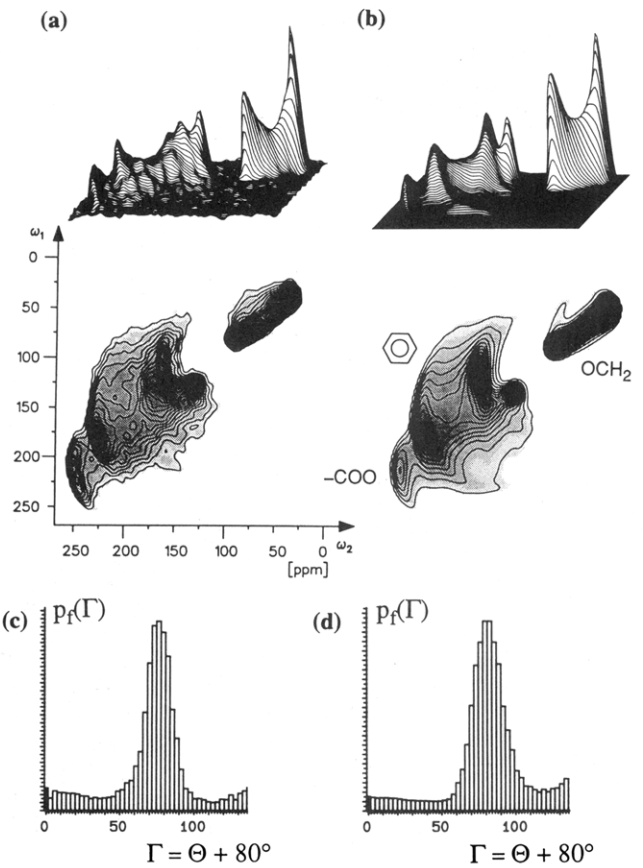

Figure 10. 2D ^{13}C DECODER spectra for a biaxial, 12-μm PET film flipped through an angle $\beta = 40°$. The experimental spectrum in (a) corresponds to an out-of-plane sample configuration (Figure 6a). (b) Five-site simulation spectrum with 15° fwhm out-of-plane disorder of the chain axes and 55° fwhm out-of-plane disorder of the planes of the phenylene rings. In addition, a 20% contribution from an isotropic powder component has been included to improve the fit, consistent also with the spectra of the same material shown below. (c) Out-of-plane distribution of OCH_2 $\mathbf{Z}_P$ axes reconstructed from the experimental spectrum in (a); the fwhm is 24°. The plot is restricted to the angular range spanning 135° where unique reconstruction is possible. (d) Distribution analogous to that in (c), reconstructed from the simulated spectrum in (b).

of the various segmental groups within the PET chains. The analyses below will use these, as well as the chemical shift values obtained from 2D DECODER measurements of bulk isotropic PET, without change to analyze quantitatively the orientational order of chains and segmental groups in thin PET films.

Biaxial PET Films. The 1D spectra of Figure 1 show that the smallest spread of intensity is observed when $\mathbf{B}_0$ is parallel to ND and thus demonstrate that in the biaxial PET films the direction characterizing the highest degree of order is the film normal ND. This makes it convenient to define ND as the sample director $\mathbf{Z}_D$ in these films and *not* one of the stretching directions MD or TD. As noted above, the width and further characteristics of the orientation distribution cannot be determined uniquely or with precision from the 1D spectra. In fact, several 2D DECODER spectra are required to analyze the complicated orientation distribution of the PET repeat unit, which must be specified in terms of the three Euler angles (Ψ_M,Θ_M,Φ_M): (i) the out-of-plane distribution of the chain axes $\mathbf{Z}_M$, in terms of Θ_M between a given chain axis and $\mathbf{Z}_D$ = ND; (ii) the out-of-plane distribution of the molecular segments *around* the chain axes $\mathbf{Z}_M$, with Ψ_M as the relevant variable; (iii) the in-plane distribution of the chain axes $\mathbf{Z}_M$, given as a function of Φ_M (here, MD can be chosen as X_D, the direction of $\Phi_M = 0$). The *out-of*-plane distribution is found to be best analyzed with the $\mathbf{B}_0$ field orientations out of the film plane, while the *in*-plane properties are best examined with the $\mathbf{B}_0$ field orientations in the plane of the film sheets. The carboxyl and OCH_2 shift tensors probe mainly the distribution aspects (i) and (iii) in the corresponding in- and out-of-plane spectra, as their nearly unique $\mathbf{Z}_P$ axes are essentially parallel to $\mathbf{Z}_M$. The phenylene rings probe in particular aspect (ii) with their $\mathbf{Z}_P$, which is perpendicular to the chain axis.

Out-of-Plane Distribution of Chain Axes $\mathbf{Z}_M$. Figure 10 displays a 2D ^{13}C DECODER spectrum ($\beta = 40°$ flip angle) for a biaxial PET film assembled in an out-of-plane configuration according to the arrangement shown in Figure 6a. The high degree of order is directly reflected in the distribution of spectral intensity, which is concentrated only in certain stripes within the range accessible in the powder spectrum (Figure 7). Of the elliptical ridges indicated in the powder spectrum, only short arcs are observed for these biaxial films. The lengths of these arcs grow with the width of the distribution of orientations. For instance, with $\eta = 0$ and a sample flip geometry of $\beta \approx 45°$, the width of the distribution in Θ is proportional to the length of the arc.[13] The distribution of $\mathbf{Z}_P$ axes in a plane containing the ND reconstructed from the spectral intensity of the OCH_2 units is displayed in Figure 10c. Due to $\Theta_M \approx \Theta$ for the methylene groups, the distribution

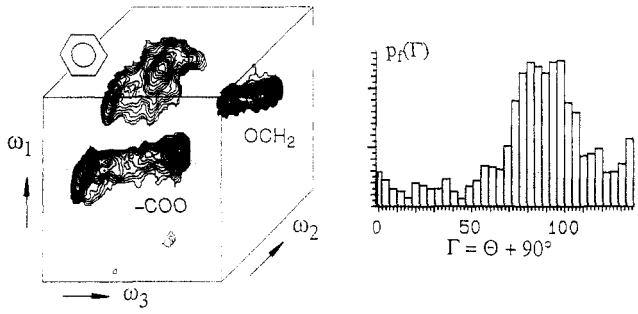

Figure 11. 3D ^{13}C DECODER spectrum for the same biaxial, 12-μm PET film sample, in an out-of-plane configuration, as used in Figure 10a, but flipped through successive angles β = +42° and β = +42° during the mixing time. The normals of the planes of the films were positioned nearly parallel to the $\mathbf{B}_0$ field during the first evolution period; thus, the ω_1 projection is similar to the 1D spectrum of Figure 1b, achieving separation of four carbon sites. To the right: Out-of-plane distribution of carboxyl $\mathbf{Z}_P$ axes reconstructed over a range of 135° from the carboxyl pattern; the fwhm is 38°. The 3D spectrum was acquired using 48 h of measurement time, with 40 t_2 increments and 20 t_1 increments.

in Θ is nearly equal to the desired Θ_M distribution. The width of the experimentally obtained distribution, about 20°, is the upper limit for the width of the Θ_M distribution; the best value for the overall simulation shown in Figure 10d was found to be 15°.

The carboxyl pattern, which has the potentially highest angular resolution, extends out of the region where it overlaps the phenylene patterns into the low-field end of the spectrum, such that a portion of its ellipse can be detected. From the length of this arc, if sufficiently distinct from the phenylene patterns, the value of $\Delta\Theta_M$ for the carboxyl sites can be determined. To perform a convincing direct reconstruction on the carboxyl pattern and as a proof of the validity of the spectral analysis, the carboxyl pattern was separated from the phenyl patterns by extending the DECODER experiment into a third dimension.[10] This is accomplished by sandwiching another evolution time, a second mixing time with sample flip, and the corresponding storage and restoration pulses into the experiment. With the main sample orientation direction (ND for the biaxial films) along the $\mathbf{B}_0$ field in the first evolution time, the overlapping patterns can usually be separated along the third frequency dimension. A 3D DECODER experiment employing two successive β = 42° flip angles resolves the previously overlapping carboxyl and phenyl patterns, as shown in Figure 11. From the carboxyl pattern, the out-of-plane distribution of carboxyl group $\mathbf{Z}_P$ axes was determined to be 35 ± 5°. As an even more powerful possibility (discussed above), 3D DECODER NMR provides in principle an avenue to the full three-dimensional distribution $P(\Psi,\Theta,\Phi)$ of molecular segments in the sample.

Out-of-Plane Disorder around Chain Axes $\mathbf{Z}_M$. The out-of-plane disorder of the molecular segments around $\mathbf{Z}_M$ is reflected in the phenyl patterns and to some extent in the carboxyl pattern. With our choice of $\mathbf{Z}_D$ = ND, a Θ value measured in the DECODER spectrum is directly related to the out-of-plane angles Ψ_M and Θ_M of the molecular segment. Ψ_M is the quantity of interest here, so we set Θ_M = 90°. With the unique principal axis $\mathbf{Z}_P$ making an angle β_P with the chain direction $\mathbf{Z}_M$, we then have

$$\cos\Theta = \sin\beta_P \sin\Psi_M \qquad (14)$$

as can be derived from the scalar product $\cos\Theta = \mathbf{Z}_P \cdot \mathbf{Z}_M$. If β_P = 0°, according to eq 14 we have Θ = 90° independent of Ψ_M: β_P = 0° and Θ_M = 90° mean that the principal axis $\mathbf{Z}_P$ is perpendicular to the sample director $\mathbf{Z}_D$ regardless of Ψ_M. For β_P = 90°, we have $\Theta = 90° - \Psi_M$: the principal axis $\mathbf{Z}_P$ is perpendicular to the chain axis $\mathbf{Z}_M$, so that the rotation by Ψ_M around $\mathbf{Z}_M$ has the maximal effect in the DECODER spectrum.

For the carboxyl and OCH_2 groups, with η relatively close to zero and β_P being small, the spectra are not particularly sensitive to the out-of-plane disorder around $\mathbf{Z}_M$; for β_P = 18° and $\Delta\Psi_M$ = 55°, the resulting spread in Θ is only about 15° according to eq 14. The $\mathbf{Z}_P$ axis of the phenylene carbons, on the other hand, exhibits β_P = 90°. (In spite of $\eta \neq 0$ here, the above arguments can still be applied qualitatively.) Therefore, the phenylene carbons probe the out-of-plane disorder around the chain axis in a sensitive fashion, so that the disorder can be estimated quite directly from the phenylene arc patterns in the DECODER spectrum of Figure 10a.

In summary, the best fit of the out-of-plane spectrum yields central angles $\langle\Theta_M\rangle$ = 90° and $\langle\Psi_M\rangle$ = 0°, as well as widths of $\Delta\Theta_M$ = 15° (±10° error margin) and $\Delta\Psi_M$ = 55° (±10°). This means that the chain tilt relative to the plane of the sheet is small and that the planar segments are preferentially, but not quite as perfectly, parallel to the film plane. From the distribution thus established, the order parameters can be determined according to eq 6. The resulting values for the highly oriented component and for the full distribution, including the disordered component, are listed in Table III.

In-Plane Distribution of Chain Axes $\mathbf{Z}_M$. Figure 12a displays the 2D DECODER spectrum (β = 40°) of the same biaxial PET film discussed above, but for an in-plane sample configuration (cf. Figure 6b). Characteristic ellipses are resolved for the carboxyl, OCH_2, and phenylene carbons. Similar to Figure 10a, the OCH_2 species are fully resolved in the upper right-hand (upfield) corner of the 2D spectrum, as the projection onto the ω_2 axis in both cases corresponds to the spectrum of Figure 1a. The carboxyl and phenylene carbons occupy similar spectral regions. The latter, however, are quite clearly distinguished for the in-plane configuration: the carboxyl signals surround those of the phenylene sites. More importantly, the variations in the signal intensities around the rings are a sensitive measure of sample biaxiality, specifically, of the distribution of $\mathbf{Z}_P$ axes in the plane of the films. This distribution as extracted directly from the OCH_2 spectrum is plotted in Figure 12c with that obtained from the simulated spectrum (Figure 12b) appearing in Figure 12d. It reflects essentially the distribution of chain axes in the plane of the sheets, since $\mathbf{Z}_P$ is parallel to $\mathbf{Z}_M$ within 8°. The width of the curve is approximately 90° in terms of Φ. Consistent with this, the fit of the five-site simulation, Figure 12b, was obtained using $\Delta\Phi_M$ = 85° (±10°). The curve can be measured over a range of 180° and has been repeated once to produce a plot through 360°. This representation makes it much easier to recognize the features of the distribution of the chains in the plane of the film. Note that the approximate symmetry with respect to the maximum of the distribution was not contrived or input but is a direct result of the reconstruction. The corresponding distribution of the carboxyl $\mathbf{Z}_P$ axes is shown in Figure 12e, showing a similar distribution as the carboxyl $\mathbf{Z}_P$ axes, possibly with a smaller contribution of segments perpendicular to the preferred direction. Figure 12f displays the distribution of carboxyl $\mathbf{Z}_P$ axes as determined from the accompanying simulation.

From the full simulations of the spectra, it must be concluded that the high "background" in the in-plane

Table III
Order Parameters of the Orientation Distributions Determined for the PET Samples in This Study[a]

Biaxial PET Films (with ND as the Z_D Axis)

	order parameter						
	$\langle D_{200}\rangle$	$\langle D_{202}\rangle$	$\langle D_{220}\rangle$	$\langle D_{222}\rangle$	$\langle D_{400}\rangle$	$\langle D_{402}\rangle$	$\langle D_{420}\rangle$
overall	−0.38	−0.14	0.26	−0.04	0.26	0.08	−0.17
oriented component	−0.48	−0.18	0.36	−0.05	0.33	0.10	−0.21

	order parameter						
	$\langle D_{422}\rangle$	$\langle D_{440}\rangle$	$\langle D_{600}\rangle$	$\langle D_{602}\rangle$	$\langle D_{620}\rangle$	$\langle D_{640}\rangle$	$\langle D_{800}\rangle$
overall	−0.03	0.09	−0.19	−0.06	0.12	−0.05	0.14
oriented component	−0.04	0.11	−0.24	−0.08	0.15	−0.06	0.17

	order parameter						
	$\langle D_{802}\rangle$	$\langle D_{820}\rangle$	$\langle D_{10,0,0}\rangle$	$\langle D_{10,0,2}\rangle$	$\langle D_{10,2,0}\rangle$	$\langle D_{12,0,0}\rangle$	$\langle D_{12,2,0}\rangle$
overall	0.04	−0.09	−0.10	−0.03	0.06	0.07	−0.04
oriented component	0.05	−0.11	−0.12	−0.04	0.08	0.09	−0.05

Uniaxial PET Fibers

	moment						
	P_2	P_4	P_6	P_8	P_{10}	P_{12}	P_{14}
overall	0.60	0.47	0.37	0.26	0.17	0.10	0.05
oriented component	0.93	0.79	0.62	0.44	0.28	0.17	0.09

Uniaxial PET Films

moment		
P_2	P_4	P_6
0.19 ± 0.05	0.02 ± 0.005	0.002

[a] Only values exceeding 0.03 are listed. Error margins range from 0.03 to 0.05.

distributions is only partially due to unoriented material (ca. 20% in these samples). Rather, it stems from chains highly parallel to the planes of the films, but broadly distributed within the film. It is interesting to note that in WAXS patterns with these films mounted normal to the X-ray beam, little orientational ordering of the chains in the plane of the films is detected at all, while it is clearly observed in the DECODER NMR spectra. To summarize the analysis of the PET films up to this point, the main features of the orientation distribution of the highly oriented component are shown schematically in Figure 13.

In many stretched films, the machine direction represents the preferred order direction. In the biaxial PET films investigated here, however, the machine direction MD is the direction along which the *fewest* chains are aligned, consistent with the results of earlier investigations.[6,10] This is concluded directly from the spectra, without the necessity of referring to simulations. For instance, the transverse direction TD was purposely oriented parallel to the $\mathbf{B}_0$ field during the detection period of the spectrum in Figure 14a. For the OCH_2 and carboxyl carbon signals, the intensity is concentrated at $\omega_2 = \omega_z$, i.e., at the extreme ends of the spectrum, showing that in the detection period, the $\mathbf{B}_0$ field is preferentially parallel to the methylene and carboxyl $\mathbf{Z}_P$ principal axes. These are in turn parallel to their respective chain axis within 20°. This means that approximately TD $\parallel \mathbf{B}_0 \parallel \mathbf{Z}_P \parallel \mathbf{Z}_M$; i.e., the chain axes $\mathbf{Z}_M$ are preferentially aligned along the transverse direction.

In addition to the dominating, relatively highly oriented fraction of chains analyzed so far, the spectra of the biaxial films also contain contributions of a component with a very broad distribution of orientations. This is consistent with the nearly rotationally invariant spectral component detected in the 1D spectra of Figure 1c,d. In the 2D simulations, this component could be approximated as isotropic. It makes up 20 ± 10% of the sample. With a crystallinity of ca. 40%, we can conclude that about 40% of the sample must be made up of quite highly oriented noncrystalline regions. This argument stipulates that cross-polarization efficiency in these regions is not significantly reduced. This is actually a reasonable assumption, since the spectra with single-pulse-excitation in Figure 1c,d show that molecular mobility in the disordered regions is anisotropic in character: Isotropic motion would leave only peaks at the isotropic chemical shift positions of the four sites in PET.

The moments of the orientation distributions for the biaxial films are listed in Table III. The results for the center are in good agreement with some moment values determined by Henrichs,[10] if the necessary changes of indices and labeling of axes are made. However, it is important to note that the moments do not reflect a single Gaussian distribution, but rather result from the superposition of a nearly isotropic fraction and (a majority of) chains that are highly ordered in certain planes, as is indicated by the second row in Table III.

It is interesting to compare these results with those obtained by Röber and Zachmann[9] on deuterated PET films. They performed a detailed analysis of the orientation behavior of PET films 220 μm thick by means of ^2H lineshape fitting, exploiting also differences in relaxation times to distinguish different fractions in the samples. Our results agree with the ^2H NMR study in finding that noncrystalline regions making up 30–40% of the sample show similar orientational properties as the crystalline components.

Order in Different Regions of a Biaxial Film. The enhanced resolution of the multidimensional frequency presentation in the DECODER experiment provides numerous opportunities for examining problems of practical importance. DECODER NMR on ^{13}C in natural abundance can be applied to industrial materials, including

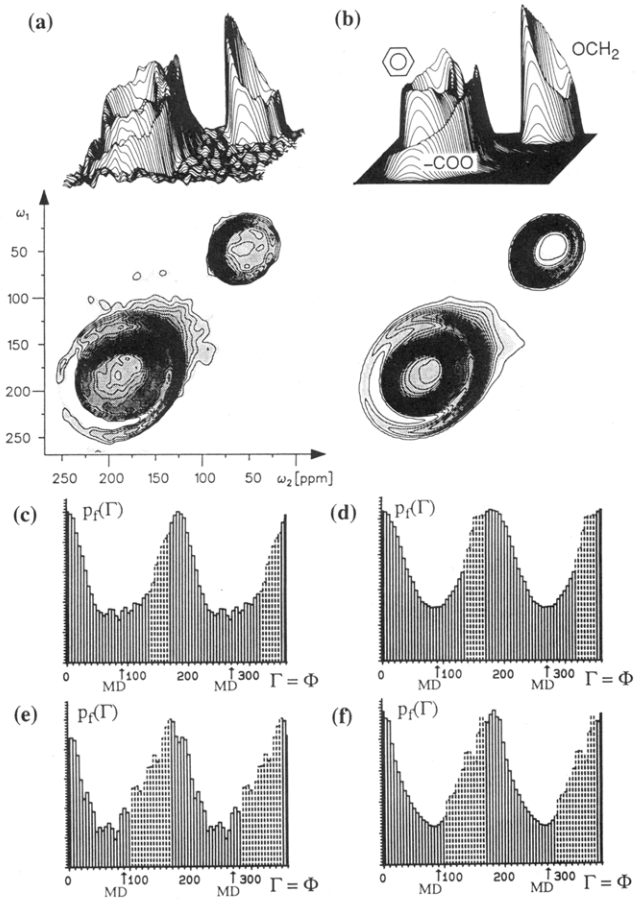

Figure 12. (a) 2D ^{13}C DECODER spectrum for a biaxial, 12-μm PET film flipped through $\beta = 40°$ during t_m. An in-plane sample configuration (Figure 6b) has been used, which positions both MD and TD normal to the axis of sample rotation. (b) Five-site simulation spectrum with the same parameters as in Figure 10b. The spectrum is most sensitive to the in-plane disorder of 85° fwhm. (c) Plot of the distribution of the OCH_2 $\mathbf{Z}_P$ axes in the plane of the films as directly reconstructed from the experimental spectrum. As $\mathbf{Z}_P$ is nearly parallel to $\mathbf{Z}_M$, the plot essentially reflects the distribution of chain axes in the film plane. (d) Distribution analogous to that shown in (c), reconstructed from the simulated spectrum in (b). (e) Same as (c) for the carboxyl carbons. Due to overlap with phenylene intensity, the dashed region extends over a larger range. (f) Distribution analogous to that shown in (e), obtained from the simulation in (b).

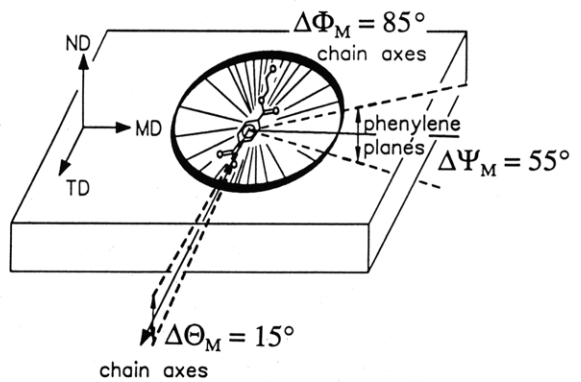

Figure 13. Schematic representation of the main features of the orientation distribution in the biaxial PET films, as obtained from the DECODER spectra and the reconstructed distributions shown above. The planes of the phenylene rings are preferentially parallel to the surfaces of the films.

those originating from actual process lines. Figure 14 contains 2D ^{13}C DECODER spectra ($\beta = 42°$ flip angle) for two biaxially ordered 12-μm PET film samples from different spatial positions across a single industrial sheet several meters wide, which has been stretched both

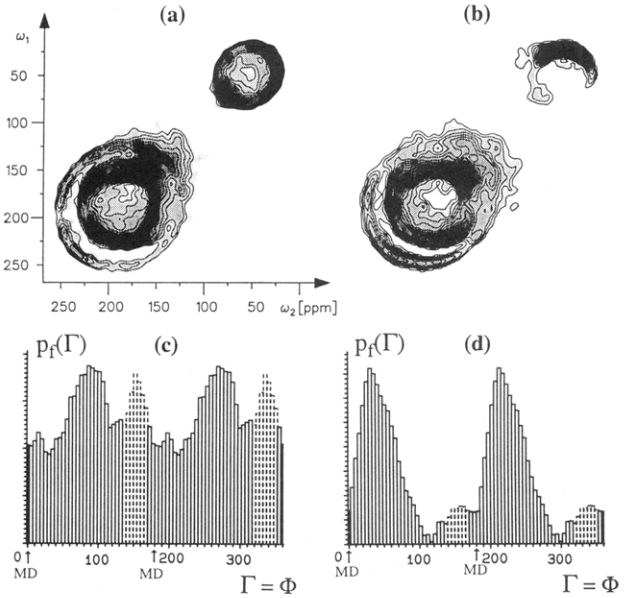

Figure 14. 2D ^{13}C DECODER spectra ($\beta = 42°$) for biaxial, 12-μm PET film samples taken from (a) the center and (b) the extreme side of a commercial sheet of PET. Both samples were prepared with identical in-plane configurations, with the transverse direction along the $\mathbf{B}_0$ field during the detection period. (c and d) Plots of the distributions of the OCH_2 $\mathbf{Z}_P$ axes in the planes of the films as directly extracted from the experimental spectra in (a) and (b). The histograms essentially reflect the distributions of chain axes in the planes of the sheets. The peak in the dashed region in (c) is due to overlap from the spectral maximum of the disordered component.

longitudinally and transversely. Both samples have been assembled in identical in-plane configurations (Figure 6b), with the normal direction ND aligned parallel to the axis of rotation. The spectrum in Figure 14a was obtained from a sample taken from the center of the main PET process sheet, whereas that in Figure 14b comes from a sample acquired from the extreme side of the same sheet at the same longitudinal position. The spectra for the two samples both exhibit the elliptical ridge patterns seen in Figure 12, but differ appreciably in their intensity distributions around the rings. A significantly higher degree of order is observed in the sample from the sheet side. This is particularly clear in the OCH_2 frequency pattern, which reveals a much narrower distribution of frequencies around the ellipse in the sample from the edge (Figure 14b), reflecting a substantially narrower distribution of the chains within the sheet. A rotation of the preferential orientation can immediately be read from the spectra and the corresponding reconstructed in-plane distributions for the center and side sheet (Figure 14c,d). They show that the maximum of the distribution is rotated by 45 ± 10° toward the machine direction. This is consistent with separate measurements of the rotation of the refractive-index ellipsoid by 35 ± 5°. The pronounced difference in the shape of the distribution is consistent with WAXS measurements with the X-ray beam perpendicular to the planes of the films. The higher degree of order, $\Delta\Phi_M = 55°$ (±10°) down from 90° (±15°), and the rotated director orientation possibly arise from the clamps that effect the transverse stretching: while moving alongside the film, they can be expected to exert stress along the MD at the edge of the sheet. Note that the biaxial frequency pattern of the OCH_2 groups is nearly identical to that portrayed in Figure 5c.

Uniaxially Drawn PET Films. A longitudinally drawn 65-μm PET film sample, which represents the starting material for the biaxial films, was also investigated

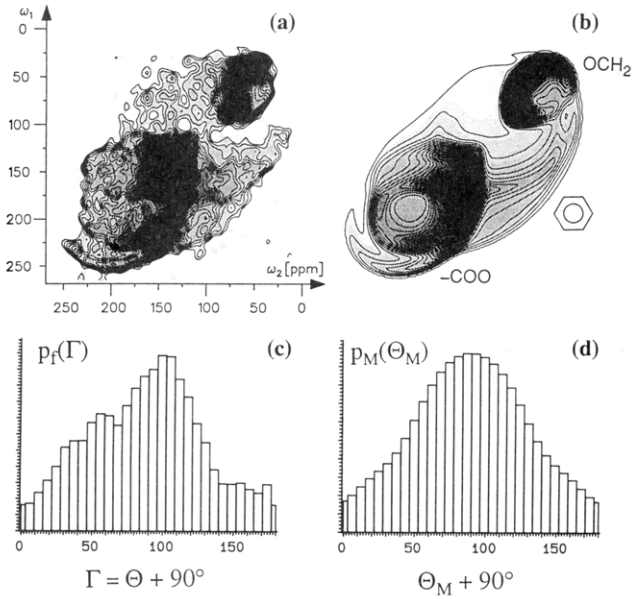

Figure 15. (a) 2D ^{13}C DECODER spectrum and simulation for a uniaxial, 65-μm PET film flipped through an angle $\beta = 40°$ during the mixing time. The spectrum corresponds to an in-plane sample configuration with the machine direction aligned normal to the axis of sample rotation. (b) Five-site simulation spectrum using the same parameters as in Figure 8 except for a fwhm of 85° in the distribution in Θ; in the initial sample orientation, $\mathbf{Z}_D$ was perpendicular to $\mathbf{B}_0$. (c) Reconstructed distribution of OCH_2 $\mathbf{Z}_P$ axes, combining data from two experimental DECODER spectra. (d) Distribution of chain axes obtained by transformation of the distribution in (c). Since only even-order moments are taken into account, the distribution is symmetrized.

by DECODER NMR. Figure 15a contains a spectrum with the $\mathbf{B}_0$ field orientations in the plane of those sheets (rotation around ND, Figure 6b). The intensity distributions observed here are broader than those in the spectra for the biaxial samples, but still exhibit characteristic deviations from the powder spectrum shown in Figure 7. The phenylene intensity patterns support a uniaxial orientation distribution. The spectrum is reproduced in the simulation (Figure 15b) with a full-width-at-half-maximum of $\Delta\Theta_M = 85°$ (±10°) for the uniaxial distribution around MD, assuming transverse isotropy. The width of the distribution is confirmed in the reconstructed distribution $p_f(\Gamma)$ shown in Figure 15c, from which upon transformation (and thereby symmetrization) $p_M(\Theta_M)$ in Figure 15d is obtained. The corresponding second moment, P_2, of the distribution for this material is only ca. 0.2. This demonstrates that the DECODER method can be applied to relatively weakly oriented materials if the signal-to-noise ratio is sufficient.

It should be appreciated that equivalent flip geometries, with rotation by 40° around the ND, produce spectra for the uniaxial and biaxial samples, Figures 15 and 12, that look so markedly different. The reason lies of course with the different orientational properties. In the case of the uniaxial sample, MD is the order axis, and for the carboxyl and OCH_2 groups, $\langle\Theta\rangle \approx \langle\Theta_m\rangle$, with both being relatively close to zero. In the biaxial films, ND is the dominant order axis, with respect to which $\langle\Theta\rangle \approx \langle\Theta_m\rangle \approx 90°$. In the former case, the order axis $\mathbf{Z}_D$ is perpendicular to the rotation axis $\mathbf{F}$, whereas in the latter it is parallel to $\mathbf{F}$.

In summary, we can say that for the carboxyl and OCH_2 groups under these flip and orientation conditions, ordered arrangement of the segments perpendicular to ND compresses the intensity into the elliptical ridge, while disorder around MD spreads the intensity along this ridge.

^2H NMR spectra of uniaxial cold-drawn deuterated PET films[9] suggest that the chain axis is not parallel to the MD. In our sample, due to the large width of the distribution of orientations, the difference between the orientation distribution (of the sample director) being centered on the chain axis or on the phenylene ring axis is marginal both physically and spectrally. The deuteron spectra exhibit no preferential ordering of phenylene ring planes in the film plane, and this is consistent with our spectra of the uniaxial films.

For analysis of even lower degrees of order, other NMR experiments may be better suited, as they detect deviations from cylindrical symmetry.[12]

V. Summary and Outlook

The principal objective of the DECODER method is to provide quantitative information on molecular orientations in solids. The method is particularly advantageous for elucidating details of complicated types of orientation distributions in samples with intermediate to high degrees of order. Probing numerous sites with good angular resolution, the DECODER technique provides results that are complementary to other methods, such as WAXS, ^2H NMR, or ^{13}C MAS NMR. As demonstrated by the PET thin film and fiber experiments on ^{13}C in natural abundance presented here, expensive or inconvenient isotopic enrichment procedures are unnecessary, allowing materials originating directly from laboratory or industrial process lines to be examined. By exploiting different sample orientations and flip angles, complicated orientation distributions can be elucidated and even reconstructed to a considerable extent.

In this paper, we have demonstrated the DECODER method on various industrial PET thin films and fiber. In drawn PET fibers, the angle between the chain axis and the phenylene axis was determined to be $\alpha_0 = 18 \pm 4°$, and the fwhm of the distribution of orientations to be $20 \pm 5°$, with a 40% contribution from a much more disordered component (fwhm $135 \pm 45°$).

In industrial biaxially drawn PET films, the chain axes are, as expected, found to be forced into the planes of the sheets. In addition, planar segments are observed to align preferentially parallel to the plane of the films. These are the two major orientational effects in the biaxial films. Two types of out-of-plane disorder can thus be distinguished: the out-of-plane disorder of the phenylene rings around the chain axis exhibits a fwhm of 55° (±10° error margin), while the tilt of the chain axes relative to the plane of the sheets is small (fwhm of $15 \pm 5°$). The spread of the chain axes within the plane could be determined in particular detail: 90° (±15°) in the center-sheet film, and 55° (±10°) in the film from the sheet edge. The transverse direction is found to be the preferential in-plane order direction for the film in the sheet center. At the edge, the sample director is found to be rotated toward the machine direction, in accordance with birefringence data. In these films, a contribution from a 20% disordered fraction is observed in the 2D DECODER spectra and in 1D experiments where selection was achieved based on differences in NMR relaxation times. In a uniaxial PET film sample, the orientation distribution of the chains is 85° (±15°) wide.

Partial overlap of frequency patterns of different ^{13}C sites in two dimensions can be more completely overcome by incorporating a second flip and a second evolution period to extend the methodology into a third dimension. Besides offering the possibility of separating frequency components, 3D DECODER NMR provides the powerful

opportunity to define the full three-dimensional orientational distribution $P(\Psi,\Theta,\Phi)$ of molecular segments in the sample. This avenue is currently under investigation in our laboratories.

Acknowledgment. We are grateful to Dr. M. Bausch-Koenig, Dupont Luxembourg, for providing the PET films and for valuable discussions. We extend our thanks to M. Hehn for construction of the double-resonance NMR probehead and the sample flipping mechanism, to M. Wilhelm for his help with the PET fiber samples, and to P. Blümler for assistance with the gray-scale plot programming. B.F.C. acknowledges the U.S. National Science Foundation for support as a NSF–NATO postdoctoral fellow. Financial support from the Deutsche Forschungsgemeinschaft (Leibniz program, SFB 262) is gratefully acknowledged.

References and Notes

(1) Ward, I. M., Ed. *Structure and Properties of Oriented Polymers*; Applied Science Publishers: London, 1975.
(2) Ward, I. M., Ed. *Developments in Oriented Polymers*; Applied Science Publishers: London, 1982; Vol. 1.
(3) For review, see: Baltá-Calleja, F. J.; Vonk, C. G. *X-Ray Scattering of Synthetic Polymers*; Elsevier: Amsterdam, 1989.
(4) Daubeny, R. de P.; Bunn, C. W., Brown, C. J. *Proc. R. Soc. London* **1954**, *226A*, 531.
(5) Hall, I. H. In *Structure of Crystalline Polymers*; Hall, I. H., Ed.; Elsevier Applied Science: London, 1984.
(6) Jungnickel, B.-J. *Angew. Makromol. Chem.* **1980**, *91*, 203; **1984**, *125*, 121.
(7) Spiess, H. W. In *Developments in Oriented Polymers*; Ward, I. M., Ed.; Applied Science Publishers: London, 1982; Vol. 1, pp 47–78 and references therein.
(8) Boeffel, C.; Spiess, H. W. In *Side Chain Liquid Crystal Polymers*; McArdle, C. B., Ed.; Blackie Publishing Group: Glasgow, 1988.
(9) Röber, S.; Zachmann, H. G. *Polymer* **1992**, *33*, 2061.
(10) Henrichs, P. M. *Macromolecules* **1987**, *20*, 2099.
(11) Hentschel, R.; Sillescu, H.; Spiess, H. W. *Polymer* **1981**, *22*, 1516.
(12) Harbison, G. S.; Vogt, V.-D.; Spiess, H. W. *J. Chem. Phys.* **1987**, *86*, 1206.
(13) Schmidt-Rohr, K.; Hehn, M.; Schaefer, D.; Spiess, H. W. *J. Chem. Phys.* **1992**, *97*, 2247.
(14) Carter, C. M.; Alderman, D. W.; Grant, D. M. *J. Magn. Reson.* **1985**, *65*, 183.
(15) Carter, C. M.; Alderman, D. W.; Grant, D. M. *J. Magn. Reson.* **1987**, *73*, 114.
(16) Jeener, J.; Meier, B. H.; Bachmann, P.; Ernst, R. R. *J. Chem. Phys.* **1979**, *71*, 4546.
(17) Schmidt, C.; Blümich, B.; Wefing, S.; Spiess, H. W. *Chem. Phys. Lett.* **1986**, *130*, 84.
(18) Schmidt, C.; Blümich, B.; Spiess, H. W. *J. Magn. Reson.* **1988**, *79*, 269.
(19) Hagemeyer, A.; Schmidt-Rohr, K.; Spiess, H. W. *Adv. Magn. Reson.* **1989**, *13*, 85.
(20) Schaefer, D.; Spiess, H. W.; Suter, U. W.; Fleming, W. W. *Macromolecules* **1990**, *23*, 3431.
(21) Haeberlen, U. *High Resolution NMR in Solids (Advances in Magnetic Resonance*, Supplement 1); Academic Press: New York, 1976.
(22) Spiess, H. W.; Schmidt-Rohr, K. *Multidimensional Solid-State NMR and Polymers*; Academic Press: London, 1993.
(23) Hughes, C. D.; Sherwood, M. H.; Alderman, D. W.; Grant, D. M. *J. Magn. Reson.*, in press.
(24) Hagemeyer, A.; Brombacher, L.; Schmidt-Rohr, K.; Spiess, H. W. *Chem. Phys. Lett.* **1990**, *167*, 583.
(25) Roe, R.-J. *J. Appl. Phys.* **1965**, *36*, 2024.
(26) Hentschel, R.; Schlitter, J.; Sillescu, H.; Spiess, H. W. *J. Chem. Phys.* **1978**, *68*, 56.
(27) Jarvis, D. A.; Hutchinson, I. J.; Bower, D. I.; Ward, I. M. *Polymer* **1980**, *21*, 41.
(28) Rose, M. E. *Elementary Theory of Angular Momentum*; John Wiley: New York, 1957.
(29) Spiess, H. W. *NMR Basic Princ. Prog.* **1978**, *15*, 55.
(30) Kilian, H. G.; Halboth, H.; Jenckel, E. *Kolloid Z. Z. Polym.* **1960**, *172*, 166.
(31) Fakirov, S.; Fischer, E. W.; Schmidt, G. F. *Makromol. Chem.* **1975**, *176*, 2459.
(32) du Bois Murphy, P.; Taki, T.; Gerstein, B. C.; Henrichs, P. M.; Massa, D. J. *J. Magn. Reson.* **1982**, *49*, 99.
(33) Veeman, W. S. *Prog. NMR Spectrosc.* **1984**, *16*, 193.
(34) Wehrle, M.; Hellmann, G. P.; Spiess, H. W. *Colloid Polym. Sci.* **1987**, *265*, 815.
(35) Hansen, M. T.; Blümich, B.; Boeffel, C.; Spiess, H. W.; Morbitzer, L.; Zembrod, A. *Macromolecules* **1992**, *25*, 5542.
(36) Schmidt-Rohr, K.; Wilhelm, M.; Johansson, A.; Spiess, H. W. *Magn. Reson. Chem.*, submitted.
(37) Arnott, S.; Wonacott, A. J. *Polymer* **1966**, *7*, 157.
(38) Wilhelm, M.; Schmidt-Rohr, K.; Spiess, H. W., unpublished results.